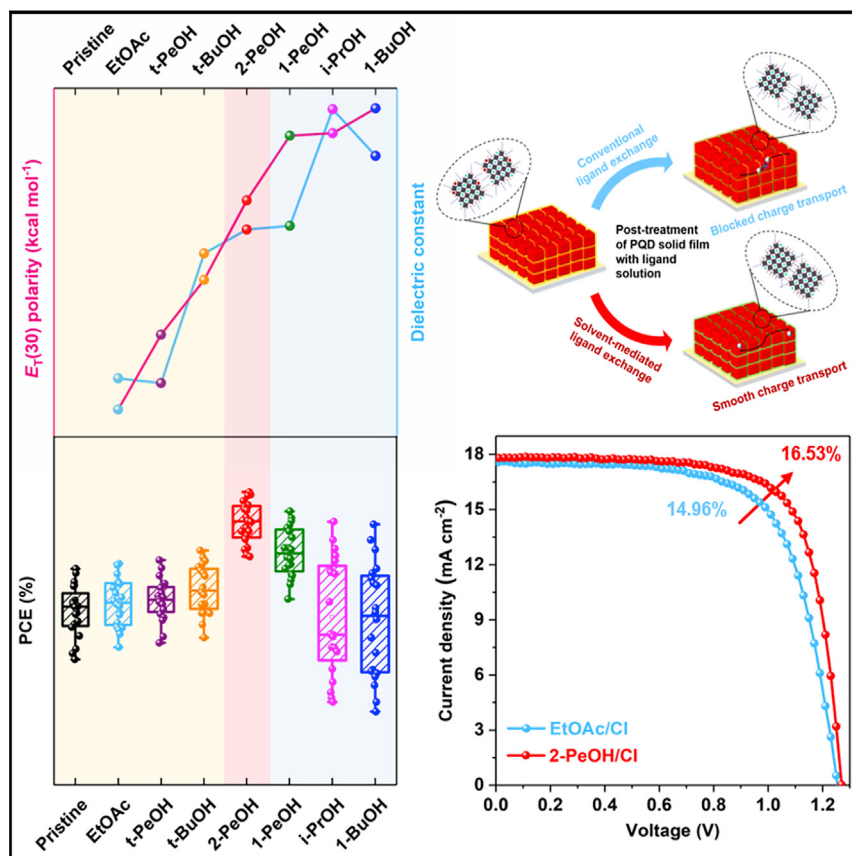


## Article

Tailoring solvent-mediated ligand exchange for CsPbI<sub>3</sub> perovskite quantum dot solar cells with efficiency exceeding 16.5%

Regulating the surface ligand chemistry of perovskite quantum dots (PQDs) is of great importance for the construction of high-performing PQD solar cells (PQDSCs). Herein, the solvent of short ligands is tailored for the post-treatment of PQD solid films to maximize the removal of pristine long-chain insulating ligands from the PQD surface and then effectively passivate PQD surface. Consequently, the PQDSC delivers an efficiency of up to 16.53%, which is the highest among inorganic PQDSCs.

Donglin Jia, Jingxuan Chen,  
Junming Qiu, Huili Ma, Mei Yu,  
Jianhua Liu, Xiaoliang Zhang

xiaoliang.zhang@buaa.edu.cn

### Highlights

Tailored solvent maximizes the removal of insulating ligands from the PQD surface

Tailored solvent mediates short ligands to adequately bind to the PQD surface

Solvent-mediated ligand exchange improves the defect passivation of PQDs

Article

# Tailoring solvent-mediated ligand exchange for CsPbI<sub>3</sub> perovskite quantum dot solar cells with efficiency exceeding 16.5%

Donglin Jia,<sup>1</sup> Jingxuan Chen,<sup>1</sup> Junming Qiu,<sup>1</sup> Huili Ma,<sup>2</sup> Mei Yu,<sup>1</sup> Jianhua Liu,<sup>1</sup> and Xiaoliang Zhang<sup>1,3,\*</sup>

## SUMMARY

Inorganic CsPbI<sub>3</sub> perovskite quantum dot (PQD) shows high potential for new-generation photovoltaics due to its outstanding optoelectronic properties. However, the binding-energy-driven ligand exchange of PQDs limits the construction of conductive and stable PQD solids for efficient PQD solar cells (PQDSCs). Herein, protic 2-pentanol with superior ligand solubility is delicately screened from massive solvents to mediate the ligand exchange of PQDs due to its appropriate dielectric constant and acidity, which could maximize the removal of pristine insulating oleylamine ligands from the PQD surface without introducing halogen vacancy defects. Employing tailored short choline ligands and 2-pentanol solvent for the post-treatment of PQD solids, PQDSC yields an efficiency of 16.53%, which is the highest among inorganic PQDSCs. This outstanding performance is attributed to the improved charge carrier transport and surface defect passivation of PQDs. This work provides a feasible platform for tuning the surface properties of PQDs and paves the way for realizing high-performing optoelectronics.

## INTRODUCTION

Inorganic cesium lead halide (CsPbX<sub>3</sub>, X = Cl, Br, or I) perovskite quantum dots (PQDs) have attracted considerable research interest due to their unique photophysical properties, such as high defect tolerance, tunable absorption and emission spectra, long carrier lifetime, and high photoluminescence (PL) quantum yields (PLQYs),<sup>1–4</sup> which make them highly potential in light-emitting diodes (LEDs),<sup>5</sup> lasers,<sup>6</sup> photodetectors,<sup>7,8</sup> and photovoltaics.<sup>9–11</sup> In particular, the PQD with CsPbI<sub>3</sub> as a constituent has enormous potential for new-generation solar cells due to its suitable band-gap energy ( $E_g$ , ~1.73 eV) and high light absorption coefficient.<sup>12</sup> Compared with the CsPbI<sub>3</sub> bulk perovskites, the preparation of CsPbI<sub>3</sub> perovskites into QDs (or nanocrystals) can improve its surface strain, leading to better stability in the black-phase ( $\alpha$ -,  $\beta$ -, or  $\gamma$ -phase).<sup>13</sup> In addition, the surface properties of PQDs can be easily tuned by controlling the surface ligands, thus making them more compatible with photovoltaic materials.<sup>14</sup> Moreover, the controllable solution-phase synthesis of PQDs avoids the severe environmental requirements of perovskite crystal growth for film deposition.<sup>15</sup> Thanks to the great efforts made in the surface chemistry,<sup>9,16,17</sup> crystal quality,<sup>10,18</sup> and compositional engineering of PQDs,<sup>19</sup> as well as the device architecture optimization of PQD solar cells (PQDSCs),<sup>20,21</sup> the power conversion efficiencies (PCEs) of CsPbI<sub>3</sub> PQDSCs were greatly boosted such that efficiencies of over 16% were reported recently.<sup>10,19</sup>

## Context & scale

The regulation of the surface ligand chemistry of perovskite quantum dots (PQDs) is critical for the construction of conductive and stable PQD solid films, thus determining the performance of PQD solar cells (PQDSCs). Taking into account the dielectric constant and acidity, we tailor the solvent of short ligands for the post-treatment of PQD solid films to remove the long-chain insulating ligands from the PQD surface without introducing halogen vacancy defects, thereby mediating a more controllable ligand exchange of PQDs. By further optimizing the short ligands with the tailored solvent environment, the resulting PQDSC achieves an efficiency of up to 16.53%, which is the highest value among inorganic PQDSCs. Our strategy provides a feasible platform to regulate the surface chemistry of PQDs for realizing high-performance optoelectronic devices.

PQDs for photovoltaic applications are generally synthesized using the hot-injection method, and long-chain oleic acid (OA) and oleylamine (OAm) ligand pairs are adopted to cap the PQD surface, making them well dispersed in the nonpolar solvent with good colloidal stability. For the deposition of PQD solid films that acted as the light absorber in the PQDSCs, a facile layer-by-layer spin-coating approach is widely employed in which the insulating OA/OAm ligands anchored on the PQD surface are supposed to be thoroughly removed or substituted by short ones, facilitating charge carrier transport within the PQD solid films. Each deposited PQD layer is rinsed with methyl acetate (MeOAc) antisolvent, thereby exchanging the pristine OA ligands with the short acetate ligands derived from the hydrolysis of MeOAc.<sup>12</sup> However, MeOAc could not thoroughly remove OAm ligands from the PQD surface due to its low dielectric constant ( $\epsilon$ ), which results in a large amount of insulating long-chain OAm ligands remaining on the PQD surface, severely impeding the charge carrier transport within the PQD solid films.<sup>22</sup> Thus, Sanehira et al. dissolved the formamidinium iodide (FAI) in ethyl acetate (EtOAc) to prepare a saturated solution, which was applied for the post-treatment of PQD solid films.<sup>23</sup> Taking advantage of conductive short FA<sup>+</sup> cations to exchange the pristine insulating OAm ligands, the charge carrier mobility within the PQD solid films was substantially improved, resulting in improved charge carrier extraction of PQDSCs. However, the intense and time-sensitive FAI ligand exchange could accelerate FA<sup>+</sup> cations penetrating perovskite lattice forming FA<sub>1-x</sub>Cs<sub>x</sub>PbI<sub>3</sub> PQDs. Moreover, the substitution of hydrophobic OAm ligands with hydrophilic FA<sup>+</sup> ligands provides access for moisture penetration, probably reducing the phase stability of CsPbI<sub>3</sub> PQDs.<sup>24</sup> Therefore, different short organic/inorganic cations used as alternative ligands were explored to substitute the pristine OAm ligands through the post-treatment of PQD solid films, which could improve the electronic coupling of inter-PQDs and simultaneously passivate the surface defects of PQDs.<sup>24,25</sup> Despite improving the performance of resulting PQDSCs to some extent by employing different short ligands, the ligand exchange determined by the intrinsic binding nature was generally unsatisfactory. Notably, the low solubility of short ligands, such as ionic salts, in the aprotic EtOAc generally causes the ligand exchange of PQDs within a saturated short-ligand solution with a very low concentration, resulting in an insufficient exchange effect. Therefore, thoroughly substituting the insulating OA/OAm ligands with short ones within an ideal solvent is highly desirable; it could further improve the photovoltaic performance and stability of PQDSCs.

Herein, a solvent-mediated ligand exchange of CsPbI<sub>3</sub> PQDs is reported to improve the ligand exchange of PQDs for high-performing solar cells. Compared with the conventional aprotic EtOAc, protic alcohols with higher dielectric constants and good solubility of short ligands were applied for the ligand exchange of PQDs during the post-treatment of PQD solid films. The results of solvent screening revealed that 2-pentanol (2-PeOH) was an ideal solvent to mediate the ligand exchange of PQDs due to its appropriate dielectric constant and acidity, which could to a large extent remove pristine insulating OAm ligands from the PQD surface without introducing halogen vacancy defects. Through using tailored choline iodide (CI) short ligands and 2-PeOH solvent for the ligand exchange of PQDs, the conductivity, optoelectronic properties, and stability of PQD solid films were substantially improved. Consequently, the PCE of PQDSCs was increased up to 16.53% (steady power output efficiency of 15.68%), which is the highest efficiency obtained among inorganic PQDSCs. The outstanding photovoltaic performance was attributed to the significantly diminished charge carrier recombination of PQDSCs, resulting from the promoted charge carrier transport within the PQD solid films and the effective surface defect passivation of PQDs. Finally, extensive theoretical calculations were

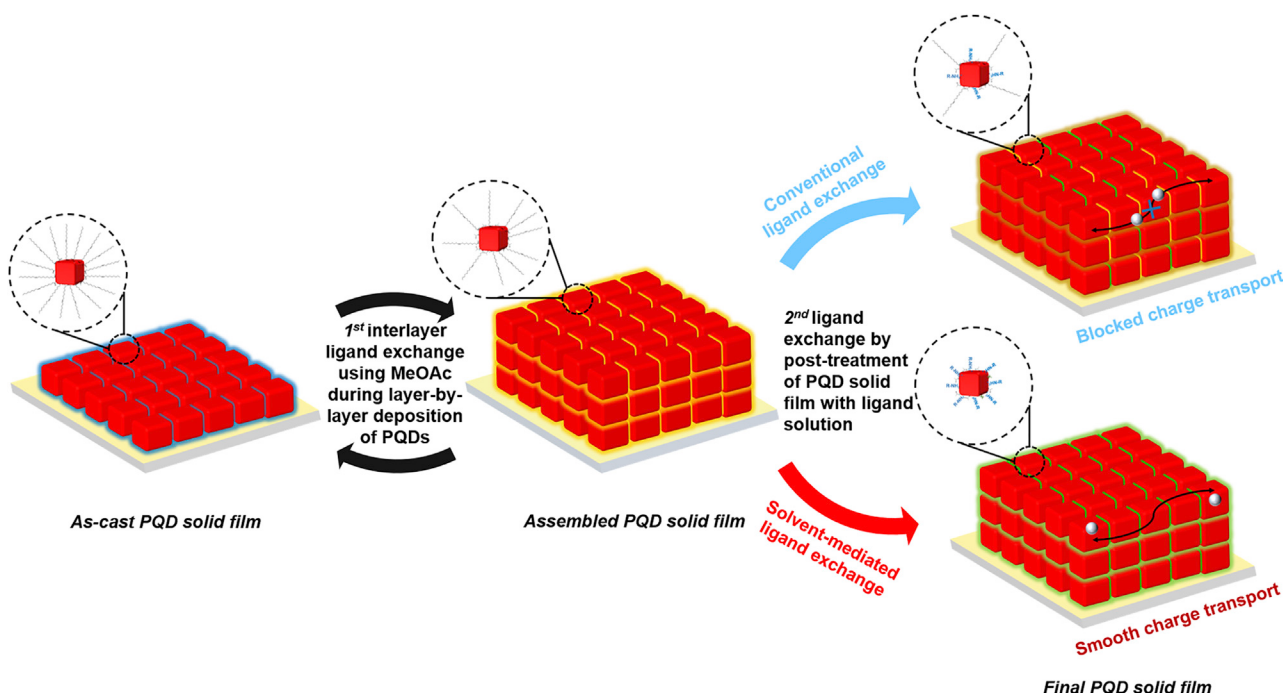
<sup>1</sup>School of Materials Science and Engineering, Beihang University, Beijing 100191, China

<sup>2</sup>Key Laboratory of Flexible Electronics (KLOFE) & Institute of Advanced Materials (IAM), Nanjing Tech University, Nanjing 211816, China

<sup>3</sup>Lead contact

\*Correspondence:  
[xiaoliang.zhang@buaa.edu.cn](mailto:xiaoliang.zhang@buaa.edu.cn)

<https://doi.org/10.1016/j.joule.2022.05.007>



**Scheme 1. Deposition and post-treatment processes of PQD solid films**

Post-treatment of PQD solid films, including conventional ligand exchange within EtOAc and solvent-mediated ligand exchange.

conducted to provide more insight into the solvent-mediated ligand exchange and its effects on the surface properties of PQDs.

## RESULTS AND DISCUSSION

### Ligand exchange of PQDs

The  $\text{CsPbI}_3$  PQD with a size of  $\sim 12$  nm was synthesized using the hot-injection method, and MeOAc antisolvent was applied to purify PQDs, in accordance with the literature (Figure S1).<sup>9,10</sup> In general, the preparation of PQD solid films for solar cells requires a two-step ligand exchange approach in consonance with prioritizing the removal of pristine insulating OA and OAm ligands from the PQD surface.<sup>23</sup> Scheme 1 describes the deposition and post-treatment processes of PQD solid films of which more detailed information is included in the [experimental procedures](#). Briefly, the PQD solid film was prepared using the layer-by-layer deposition method. During the interlayer rinsing process, most of the OA ligands were substituted by the acetate ligands produced from the hydrolysis of MeOAc.<sup>22</sup> To thoroughly remove OAm ligands from the PQD surface, post-treatment of PQD solid film is essential. Conventionally, a saturated solution of short ligands in EtOAc was applied for the post-treatment of PQD solid films, which took advantage of the differences in binding energies of the pristine OA/OAm ligands and new ligands to the PQD surface.<sup>26</sup> However, in such a conventional manner, it is generally difficult to thoroughly remove the pristine ligands from the PQD surface, which may also make it difficult to accurately control the ligand exchange of PQDs.<sup>24,27</sup> The remaining long-chain ligands significantly hinder the charge carrier transport within the PQD solid films, predominantly affecting the charge carrier extraction of PQDSCs. Therefore, an ideal solvent for the ligand exchange of PQDs during the post-treatment of PQD solid films should promote the release of bound OAm ligands and remaining OA ligands without deteriorating the internal perovskite crystal of PQDs. Meanwhile, during the ligand exchange, the exposed surface sites of PQDs need

to be coordinated with the short ligands dissolved in the solvent, which will result in the good surface defect passivation of PQDs to minimize the nonradiative recombination.

#### Photovoltaic performance of PQDSCs fabricated with neat solvent post-treatments

Solvents are generally adopted as a medium for the ligand exchange of QDs, and a suitable solvent could facilitate the ligand exchange of QDs, whereas an improper one will irreversibly deteriorate the crystal of QDs.<sup>28–30</sup> To pursue a feasible solvent for the ligand exchange of PQDs during the post-treatment of PQD solid films, we first studied the effect of neat solvent post-treatments on the performance of PQD solid films and PQDSC devices. Solvent polarity is a comprehensive parameter that is affected by numerous factors and is difficult to accurately define.<sup>31,32</sup> Therefore, we first focused on the dielectric constant of the solvent, which is one of the intuitive expressions generally used to evaluate solvent polarity.<sup>33</sup> The dielectric constant highlights the effect of the electrostatic interaction between the charged QD surface ligands and the solvent on the surface properties of QDs.<sup>34</sup> During the purification and ligand exchange of QDs, the dielectric constant of solvents is a critical parameter in regulating the surface ligand chemistry of QDs, which is considered to play a similar role during the preparation of PQD solid films.<sup>35,36</sup> As the dielectric constant of the antisolvent used for the purification of CsPbBr<sub>3</sub> PQDs exceeded ~23, the monodispersed CsPbBr<sub>3</sub> PQDs would be unavailable.<sup>35</sup> For the CsPbI<sub>3</sub> PQDs with a more delicate crystal structure, the upper limit of the dielectric constant of antisolvents should be more stringent. Additionally, during the deposition of PQD solid films, the dielectric constant of the antisolvent should be not too low to prevent the dissolution of the underlying PQD layer.<sup>21</sup>

The protic solvent with dual characteristics of hydrogen bond donor (HBD) and hydrogen bond acceptor (HBA) is preferred for the treatment of PQD solid films, which could ensure the high solubility of ionic salt ligands and accelerate the desorption of long-chain pristine ligands from the PQD surface.<sup>30,37</sup> By contrast, aprotic solvents with moderate polarity may be not suitable for the post-treatment of CsPbI<sub>3</sub> PQD solid films due to the lower solubility of short ligands. Meanwhile, the partially negative oxygen, nitrogen or sulfur donors of the polar components (e.g., carbonyl, sulfoxide, amide, ether, etc.) show strong complexation with the Pb<sup>2+</sup> that may dissociate the PbI<sub>6</sub> octahedral frame of PQDs.<sup>38,39</sup> According to the solvent screening exploration, we found that the protic alcohols with dielectric constants ranging from 5 to 23 met these requirements. Therefore, based on using MeOAc to remove pristine OA ligands during the layer-by-layer deposition of PQD solid films, tert-pentanol (t-PeOH), 2-PeOH, 1-pentanol (1-PeOH), tert-butanol (t-BuOH), 1-butanol (1-BuOH), isopropanol (i-PrOH), ethanol (EtOH), and methanol (MeOH) were studied as the alternative solvents for the post-treatment of PQD solid films. Structural formulas of these solvents are shown in Figure 1A, and the dielectric constants of these solvents are summarized in the upper figure of Figure 1B and in Table S1.

For the preliminary screening of the solvents, we first prepared the as-cast PQD solid film with the PQD surface covered by OA/OAm ligands, then the sample was rinsed with MeOAc to exchange the OA ligands with acetate ligands, thereby obtaining the PQD solid film named “pristine.” In our typical experiment, we further soaked the pristine PQD solid films with the conventional EtOAc or alternative alcohols to remove the OAm ligands from the PQD surface. It is found that EtOH ( $\mathcal{E}_r = 23.8$ ) and MeOH ( $\mathcal{E}_r = 33.1$ ) instantaneously result in the degradation of PQDs, indicating

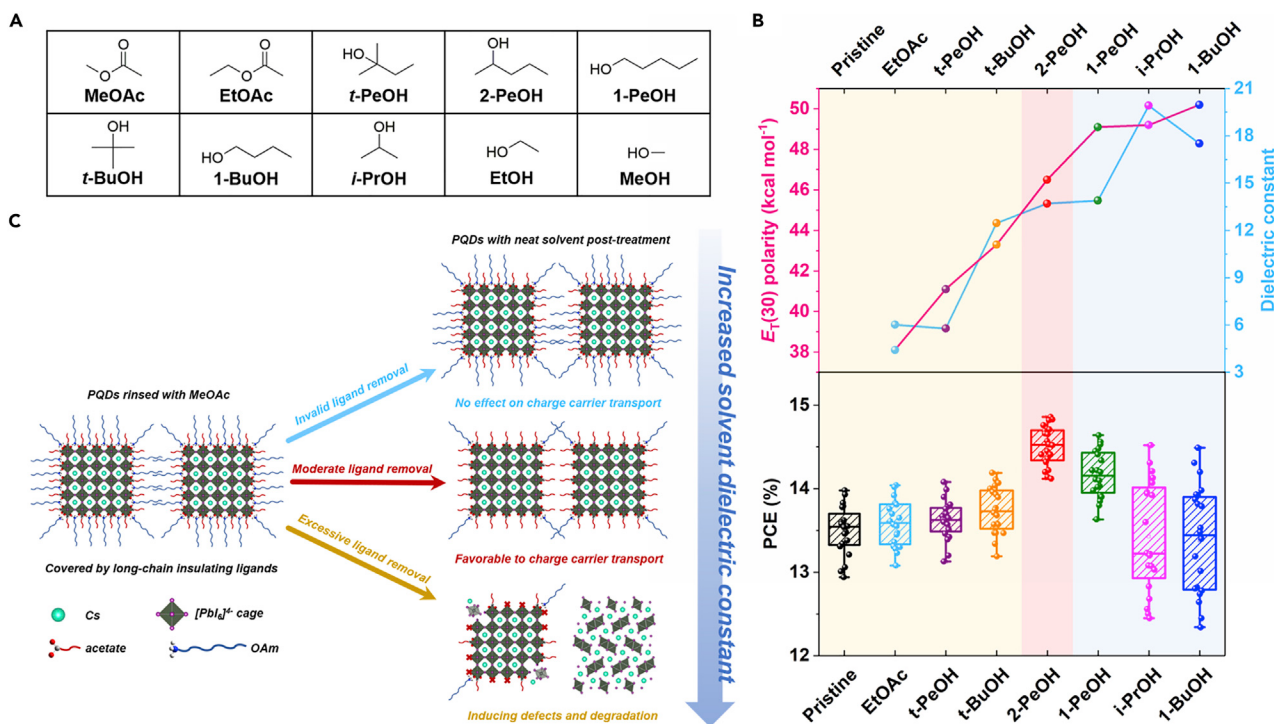


**Figure 1. Photovoltaic performance of PQDSCs fabricated with neat solvent post-treatments**

(A) Molecular structures of the alternative solvents used in this work.

(B) Diagram of  $E_T(30)$  polarity and dielectric constant values of solvents used for the post-treatment of PQD solid films (upper), and the corresponding statistical PCEs of PQDSCs fabricated with the neat solvent post-treatments (bottom). A total of 20 devices fabricated from different batches were applied for statistics.

(C) Schematic illustration of the effects of solvents with different dielectric constants on the states of PQD surface ligands during the post-treatment of PQD solid films.

that these solvents with too high dielectric constants may be not suitable for the post-treatment of PQD solid films.

To investigate the influence of neat solvent post-treatments on the photovoltaic performance of PQDSCs, we fabricated PQDSCs with a structure of indium-doped tin oxide (ITO)/SnO<sub>2</sub>/PQDs/2,2',7,7'-Tetrakis[N,N-di(4-methoxyphenyl)amino]-9,9'-spirobifluorene (Spiro-OMeTAD)/Ag, and the above available solvents were applied for the post-treatment of PQD solid films. Figure S2 presents the photocurrent density-voltage ( $J-V$ ) curves of the champion PQDSCs, fabricated with or without (w/wo) solvent post-treatments, and the photovoltaic parameters are summarized in Table S2. The pristine PQDSC gave a PCE of 13.98%, whereas a PCE of up to 14.86% was obtained in 2-PeOH-based PQDSC (Figure S3A; Table S3). The bottom figure in Figure 1B shows the statistical PCEs of these PQDSCs, which were calculated from 20 devices fabricated from different batches. Other parameters, such as open-circuit photovoltaic ( $V_{OC}$ ), short-circuit photocurrent density ( $J_{SC}$ ), and fill factor (FF) are summarized in Figure S4. It can be seen that the PQDSCs fabricated with the 2-PeOH post-treatment exhibit a higher average PCE (14.51%) than other devices. Post-treatment with the solvents with either higher or lower dielectric constants resulted in the deterioration of photovoltaic performance. In addition to using 2-PeOH for the post-treatment of the PQD solid film (Scheme 1), we also tried to treat the PQD solid film with 2-PeOH during the layer-by-layer deposition process. However, the corresponding PQDSCs showed lower performance, compared with the PQDSCs fabricated using the 2-PeOH post-treatment (Figure S3B), which

indicates that the pristine long-chain ligands still play an important role in maintaining the perovskite structure of PQDs. If the pristine ligands of PQDs are excessively removed, the perovskite structure of underlying PQD layers may deteriorate or dissolve during successive antisolvent treatments, thus deteriorating the performance of PQDSC devices.

As shown in the schematic diagram in [Figure 1C](#), the high efficiency of 2-PeOH-based PQDSCs may be attributed to the appropriate dielectric constant of 2-PeOH ( $\mathcal{E}_r = 13.71$ ), which could maximize the removal of insulating OAm ligands and avoid introducing defects on the PQD surface. The EtOAc and t-PeOH-based PQDSCs exhibit almost identical average PCEs with the pristine PQDSCs—which is probably due to their dielectric constants being too low—hardly showing any effect on the surface ligand removal of PQDs. However, when the dielectric constants of the solvents are extortionate, the corresponding PQDSCs still exhibit lower efficiencies than that of 2-PeOH-based devices, which may be due to the excessive removal of ligands, including short acetate, thus introducing more defects to the PQD surface. In addition, the photoactive black-phase PQDs are prone to degrade to unfavorable 1D orthorhombic ( $\delta$ -phase, yellow-phase) due to the excessive reduction of surface strain induced by the immoderate removal of surface ligands.<sup>13</sup>

It is notable that even though the distinct dielectric constants of solvents are likely to account for the PQDSC performance, several fundamental issues are still unexplainable. For instance, 2-PeOH and 1-PeOH possess a similar dielectric constant with a distinction of only 0.2, but the statistical PCEs of corresponding PQDSCs show an obvious difference. Besides, the statistical performance of *i*-PrOH and 1-BuOH-based PQDSCs is not completely following the changes in dielectric constants. Considering that the protic alcohols are capable to donate protons or hydrogen bonds to release carboxyl ligands from the QD surface,<sup>40</sup> we therefore introduce the HBD acidity to characterize the carboxyl dissolving ability of these solvents. It can be seen from [Table S1](#) that the HBD acidity of 1-PeOH (84) is much higher than 2-PeOH (54), which would probably result in excessive dissolving of acetate ligands from the PQD surface and thus introduce halogen (X-site) vacancy defects on the PQD surface. Similarly, compared with the 1-BuOH-based PQDSCs, the higher PCEs of *i*-PrOH-based PQDSCs could also result from the higher HBD acidity of 1-BuOH.<sup>41</sup> Therefore, the effects of the post-treatment of PQD solid films with these solvents on the performance of PQDSCs could be studied more accurately by comprehensively considering the dual effects of the dielectric constant and HBD acidity. Subsequently, we introduced Reichardt's empirical  $E_T(30)$  polarity to well balance the dielectricity and HBD acidity of the solvent.<sup>42,43</sup> A feasible way to demonstrate the  $E_T(30)$  of the solvent can be determined by using the following equation,<sup>41</sup>

$$E_T(30) \left( \text{kcal mol}^{-1} \right) = 15.2\alpha + 11.5\pi^* + 31.2 \quad (\text{Equation 1})$$

$$n = 166, r = 0.979$$

where  $\alpha$  is the HBD acidity;  $\pi^*$  is dipolarity/polarizability, suggesting the ability to stabilize a charge or a dipole by virtue of its dielectric effect;  $n$  represents the number of solvents;  $r$  stands for the correlation coefficient. It can be seen that the statistical PCEs of PQDSCs conform to the increasing trend of  $E_T(30)$  polarities of solvents as shown in [Figure 1B](#) and [Table S1](#), confirming the dielectricity and HBD acidity of the solvent jointly determine the performance of PQDSCs. Among the above available solvents, 2-PeOH may be an optimal solvent for the post-treatment of PQD solid films due to its appropriate dielectric constant and acidity.

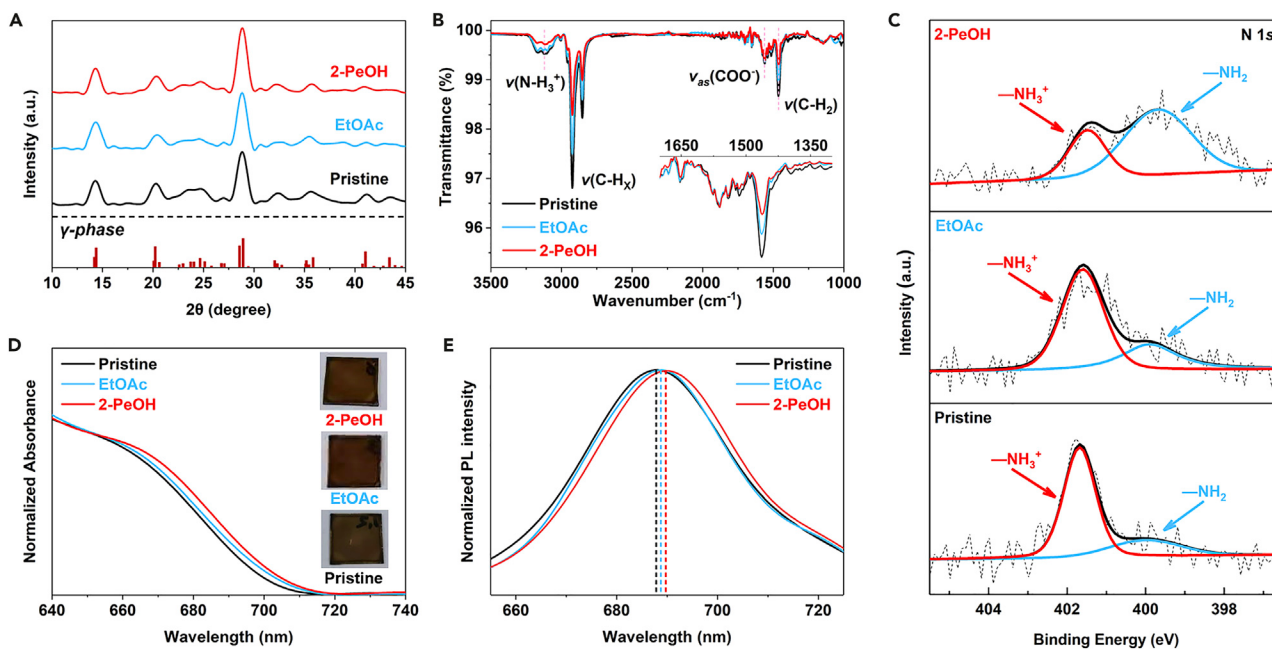


**Figure 2. Characterization of PQD solid films**

XRD patterns (A), FTIR spectra (B), N 1s core-level spectra (C), normalized light absorption spectra (D), and normalized PL spectra (E) of pristine, EtOAc, and 2-PeOH-based PQD solid films. The insets in (B) and (D) present the magnified FTIR spectra in the wavenumber range of 1,200–1,700  $\text{cm}^{-1}$  and the photographs of corresponding PQD solid films, respectively.

### Photophysical properties of PQD solid films prepared with the post-treatment

To gain more details concerning the effect of solvents on the photophysical properties of PQDs, we characterized in detail the PQD solid films prepared with different solvent post-treatments. Since the 2-PeOH shows high potential to improve the photovoltaic performance of PQDSCs, we here mainly focused on the studies of pristine, conventional EtOAc, and 2-PeOH-based PQD solid films. X-ray diffraction (XRD) patterns of the PQD solid films were measured. As shown in Figures 2A and S5A, the fresh PQD solid films prepared with the above solvent post-treatments show  $\gamma$ -phase—a widely reported photoactive black-phase in bulk perovskites and PQDs—which has a slightly distorted corner-sharing lead iodide octahedra in comparison with the  $\alpha$ -phase perovskites.<sup>13,44,45</sup> However, if the dielectric constant of the solvent was too high, such as EtOH or MeOH, the PQD was transited into  $\delta$ -phase or decomposed into lead iodide ( $\text{PbI}_2$ ) after the post-treatment (Figure S5B). We stored the PQD solid films under ambient conditions with a relative humidity (RH) of 25%–35% for 10 days and found that OA/OAm-based and pristine PQDs without the post-treatments remained the pristine  $\gamma$ -phase, whereas other PQDs with the solvent post-treatments were to some extent degraded into  $\delta$ -phase. It is worth noting that, compared with the 2-PeOH-based PQDs, the 1-PeOH-based PQDs show higher peak intensities of  $\delta$ -phase after the storage, which is probably attributed to the higher acidity of 1-PeOH that accelerates the dissolution of carboxyl ligands, thereby introducing more halogen vacancies for moisture and oxygen attacking.

Fourier transform infrared (FTIR) spectra were measured to monitor the surface ligands of PQDs (Figure 2B). For the pristine PQDs, the alkyl stretching modes ( $\nu(\text{C}-\text{H}_x)$  at 2,780–2,980  $\text{cm}^{-1}$ ,  $\nu(\text{C}-\text{H}_2)$  at 1,460  $\text{cm}^{-1}$ , and  $\nu(\text{C}=\text{C}-\text{H})$  at 3,005  $\text{cm}^{-1}$ ), carboxyl asymmetric stretching modes ( $\nu_{\text{as}}(\text{COO}^-)$  at 1,560  $\text{cm}^{-1}$ ), and ammonium stretching modes ( $\nu(\text{N}-\text{H}_3^+)$  at 3,035–3,245  $\text{cm}^{-1}$ ) could be

observed. After the post-treatment with EtOAc, the vibration intensity of the carboxyl group was unchanged, and the peak intensities of ammonium and alkyl vibrations were slightly decreased. It is notable that although EtOAc (or MeOAc) hardly removes OAm ligands from the PQD surface,<sup>22</sup> as the rinsing time increased, the OAm ligands loosely bound to the PQD surface would still become slightly detached in a weak polar environment.<sup>44</sup> By contrast, after the 2-PeOH post-treatment, the vibration intensities of alkyl and ammonium were significantly weakened and that of carboxyl remained almost constant. Since the surface ligands of pristine PQDs are mainly OAm and acetate,<sup>22</sup> after simultaneously comparing the FTIR spectra of the PQD solid films treated with different solvents, we believe that the 2-PeOH with a moderately higher dielectric constant could facilitate the removal of OAm ligands,<sup>36</sup> whereas the relatively weak acidity of 2-PeOH may inhibit it from generating excess protons, thereby restraining its dissociation of acetate ligands from the PQD surface, as demonstrated in Note S1 and Figure S6.<sup>28</sup> Furthermore, to intuitively demonstrate the ligands' removal regulations of the solvents with different dielectric constants and acidities, we dissolved PbI<sub>2</sub>, acetic acid, and OAm in 1-octadecene (ODE) to prepare the OAm and acetate ligands capped PbI<sub>2</sub> to simulate the surface state of pristine PQDs, followed by adding different solvents into the solutions to compare their phenomenon and spectra. The results are consistent with the FTIR spectra as shown in Figures 2B and S6 and demonstrated in Note S2 and Figure S7. It is worth noting that the halogen vacancy on the perovskite surface was proven to be one of the main causes for charge carrier recombination of perovskite solar cells (PSCs).<sup>46</sup> Therefore, the removal of short acetate ligands from the PQD surface could introduce more halogen vacancy defects on the PQD surface, thereby deteriorating the charge carrier transport within the PQD solid films.<sup>47</sup>

To study the composition and surface chemistry of PQDs, X-ray photoelectron spectroscopy (XPS) measurement of PQD solid films was performed. After the post-treatment with EtOAc or 2-PeOH, the peak positions of both I 3d and Pb 4f core-level spectra show ignorable changes (Figure S8), suggesting the preservation of acetate ligands on the PQD surface after the post-treatment. However, the peak positions of Cs 3d core-level spectra of EtOAc and 2-PeOH-based samples incrementally shift to lower binding energies, demonstrating that the chemical environment of A-site on the PQD surface gradually changes, likely resulting from the desorption of OAm ligands from the PQD surface.<sup>48</sup> Moreover, the spectra of N 1s core level also show noticeable changes after solvent post-treatments. As shown in Figure 2C, the N 1s core-level spectra were fitted using two components at 399.8 and 401.6 eV, respectively. The dominant peak at 401.6 eV corresponds to the ammonium group ( $\text{-NH}_3^+$ ), whereas the peak at 399.8 eV is attributed to the deprotonated amine group ( $\text{-NH}_2$ ).<sup>49</sup> The existence of two N 1s core levels indicates the dynamic equilibria from ammonium to amine states of OAm ligands, and the feature of the amine group is stronger in 2-PeOH-based PQDs in comparison with those in pristine and EtOAc-based samples. Moreover, the relative C and N contents in the 2-PeOH-based PQDs are lower than those in pristine and EtOAc-based PQDs (Table S4). These results confirm that the 2-PeOH post-treatment could effectively remove OAm ligands from the PQD surface, whereas the conventional EtOAc post-treatment hardly achieves that.

Light absorption and steady-state PL measurements were carried out to study the effect of solvent post-treatments on the optical properties of PQDs. Figures 2D and 2E show the light absorption and PL spectra of pristine, EtOAc, and 2-PeOH-based PQD solid films, respectively, and the spectra of other samples w/wo the solvent treatments are shown in Figure S9. The OA/OAm-based PQDs show a PL

emission peak at 684 nm, which redshifts to 688 nm after MeOAc rinsing (pristine PQDs), which is due to the exchange of OA ligands with acetate ligands.<sup>22</sup> After the post-treatments with the alternative solvents mentioned above, the PL emission peaks of PQDs shift to longer wavelengths of 689–693 nm in which the PL emission of PQDs with EtOAc and 2-PeOH post-treatments redshifts to 689 and 690 nm, respectively. Meanwhile, the light absorption edges also show a similar redshift. Moreover, as shown in Figure 2A, the peak positions and full width at half maximums (FWHMs) of the diffraction peaks of the (200) lattice plane of the PQDs with the solvent post-treatment are consistent with those of the pristine PQDs, indicating that there is no change in size of PQDs after the treatment.<sup>50,51</sup> Therefore, the redshift of PL emission is ascribed to the improved electronic coupling of inter-PQDs after the removal of OAm ligands.<sup>52</sup> It is notable that the effect of EtOAc and 2-PeOH on the removal of surface ligands is ignorable as the post-treating time ranges from 1 to 90 s (Figure S10). Furthermore, time-resolved PL (TRPL) decay measurement was carried out to study the carrier dynamics within the PQD solid films, and the results were fitted using a bi-exponential model (Figure S11A; Table S5). As expected, the 2-PeOH-based PQDs show a longer PL lifetime than that of pristine and EtOAc-based PQDs, which indicates that the removal of excess pristine insulating OAm ligands by 2-PeOH leads to suppressed nonradiative recombination.<sup>53–55</sup> The effect of solvent post-treatments on the carrier mobilities within the PQD solid films is quantitatively investigated using the space-charge-limited current (SCLC) measurements (Figure S11B). The calculated electron mobilities ( $\mu_e$ ) within the pristine and EtOAc-based PQD solid films are  $3.2 \times 10^{-4}$  and  $3.78 \times 10^{-4} \text{ cm}^2 \text{ V}^{-1} \text{ S}^{-1}$ , respectively. By contrast, after the post-treatment with 2-PeOH, the carrier mobility within the PQD solid film is significantly increased to  $1.93 \times 10^{-3} \text{ cm}^2 \text{ V}^{-1} \text{ S}^{-1}$ . In addition, the small differences in the trap-filled limit voltages ( $V_{TFL}$ , 0.24–0.26 V) reveal that the number of surface defects of PQDs resulting from 2-PeOH post-treatment is almost negligible, whereas the conductivity of PQD solid film is significantly improved after the 2-PeOH post-treatment (Figure S11C).

Therefore, it can be seen that the solvent post-treatment significantly affects the state of PQD surface ligands and the conductivity of PQD solid films. However, insufficient or excessive removal of ligands, using the solvents with improper dielectric constants and acidities, would deteriorate the optoelectronic properties and structural stability of PQDs. Moreover, the good solubility of ionic salts in protic 2-PeOH may further improve the effect of ligand exchange of PQDs. With these important results, we conclude that among these solvents, 2-PeOH is a desirable solvent for the post-treatment of PQD solid films.

### Photovoltaic performance of PQDSCs fabricated with solvent-mediated ligand exchange

The protic 2-PeOH is considered to provide a feasible platform for ligand exchange of PQDs to achieve high-performing solar cells. Thus, PQDSC devices were fabricated with different short ligands in 2-PeOH, including guanidinium iodide (GAI), phenethylammonium iodide (PEAI), FAI, Cl, and dimethylammonium iodide (DMAI). Among these solar cells, the device fabricated with Cl post-treatment exhibited the best photovoltaic performance (Figure S12; Table S6), and therefore we paid more attention to the PQDSCs fabricated with Cl ligands. Choline cations have been successfully applied to passivate A-site defects of perovskites to improve the efficiency and stability of PSCs.<sup>56,57</sup> Herein, we dissolved Cl ligands in 2-PeOH (named 2-PeOH/Cl) for the post-treatment of PQD solid films. For comparison, conventional EtOAc was also applied to dissolve Cl ligands (named EtOAc/Cl) for the

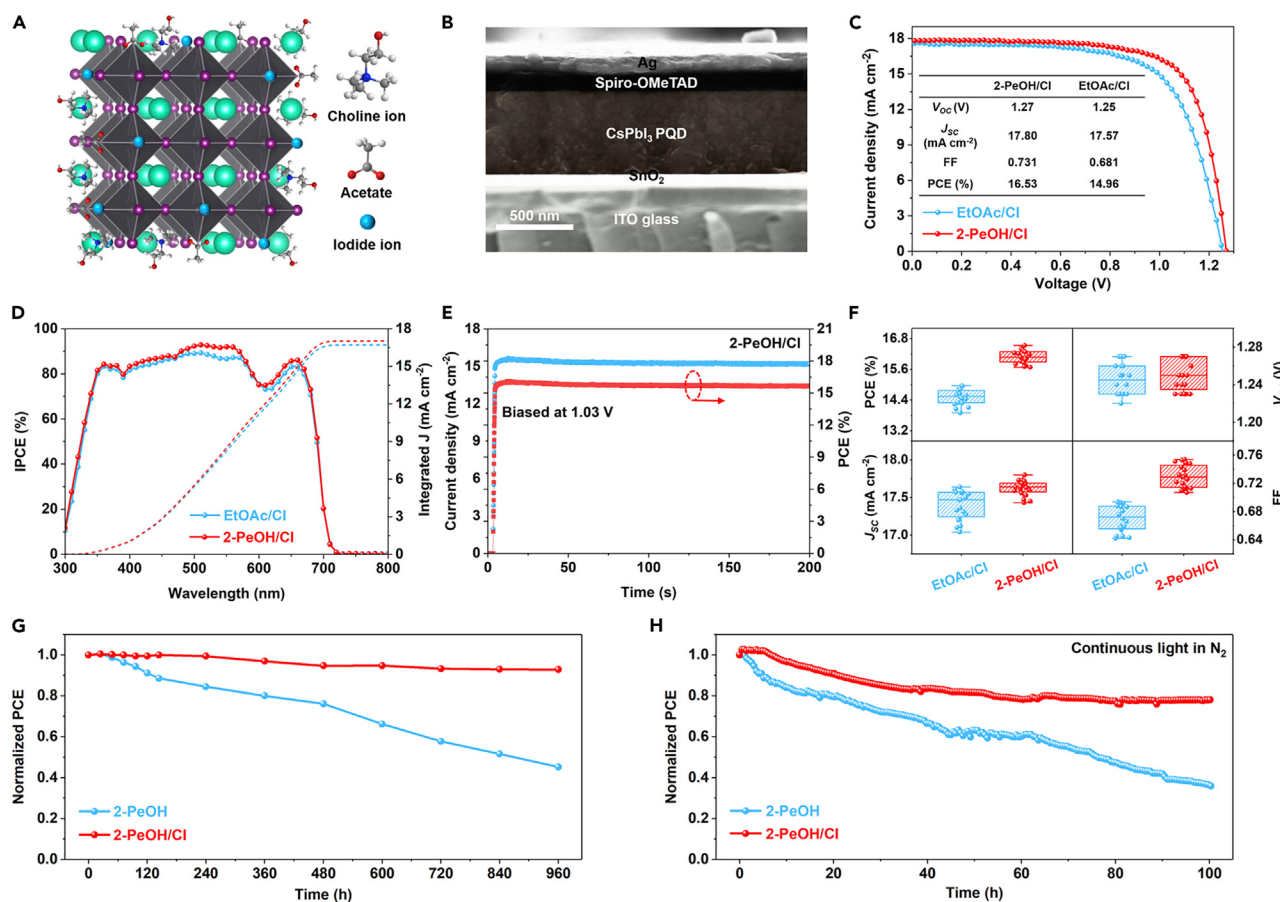


**Figure 3. Photovoltaic performance of PQDSCs fabricated with solvent-mediated ligand exchange**

(A) Proposed structural model of PQD passivated with Cl ligands.

(B) Cross-sectional SEM image of a full PQDSC device.

(C and D) J-V curves (C) and IPCE spectra and integrated photocurrent density curves (D) of EtOAc/Cl- and 2-PeOH/Cl-based PQDSCs.

(E) Stabilized current density and power output of 2-PeOH/Cl-based PQDSC measured at the maximum power point.

(F) PCE,  $V_{oc}$ ,  $J_{sc}$ , and FF statistics of EtOAc/Cl and 2-PeOH-based PQDSCs.

(G and H) Stabilities of the unencapsulated 2-PeOH and 2-PeOH/Cl-based PQDSCs under storage conditions of 5%–15% RH (G) and under continuous one sun equivalent illumination (H).

post-treatment of PQD solid films. In the proposed surface structure of the PQD, schematically displayed in Figure 3A, choline cations and iodide anions can fill the A- and X-site vacancies of the PQD surface, respectively. As shown in the FTIR spectra of EtOAc/Cl and 2-PeOH/Cl-based PQD solid films (Figure S13),<sup>58</sup> both PQDs show strong hydroxyl stretching vibrations at  $3,575\text{ cm}^{-1}$ , and other characteristics in the spectra are consistent with those of the neat EtOAc and 2-PeOH-based PQDs (Figure 2B), indicating that Cl ligands dissolved in both EtOAc and 2-PeOH were successfully bound to the PQD surface.

Figure 3B shows the cross-sectional scanning electron microscopy (SEM) image of a full PQDSC device with a planar architecture of ITO/SnO<sub>2</sub>/PQDs/Spiro-OMeTAD/Ag. Different concentrations of Cl dissolved in 2-PeOH were applied for the fabrication of PQDSCs, and the results revealed that the optimized concentration of Cl was  $0.1\text{ mg mL}^{-1}$  (Figure S14; Table S7). Notably, due to the aprotic EtOAc showing very low solubility of ionic salts, a saturated solution of Cl ( $<0.05\text{ mg mL}^{-1}$ ) in EtOAc was used for the fabrication of PQDSCs. Figure 3C shows the J-V curves of EtOAc/Cl and

2-PeOH/Cl-based PQDSCs measured under AM 1.5G 100 mW cm<sup>-2</sup> illumination. The photovoltaic performances of EtOAc/Cl and 2-PeOH/Cl-based PQDSCs are significantly improved compared with those of the corresponding neat EtOAc and 2-PeOH-based PQDSCs, likely due to the surface defect passivation of PQDs with Cl ligands. The best EtOAc/Cl-based device yielded a PCE of 14.96%. After applying 2-PeOH/Cl for the post-treatment of PQD solid films, a champion PCE of 16.53% was obtained. The higher efficiency in 2-PeOH/Cl-based PQDSCs is mainly attributed to the improved FF, likely due to the improved charge carrier extraction induced by the meliorative exchange of long-chain ligands with short ones on the PQD surface. To the best of our knowledge, such PCE is the highest value obtained among inorganic PQDSCs, as summarized in [Table S8](#). Nevertheless, we observed somewhat hysteresis when recording J-V curves under different voltage scanning directions ([Figure S15](#)), which was generally observed in the Spiro-OMeTAD-based PQDSCs, and the fundamental reasons resulting in such hysteresis remain unascertained so far.<sup>24</sup> However, the hysteresis in 2-PeOH/Cl-based PQDSC is less than that in the EtOAc/Cl-based PQDSC as a result of the decreased insulating OAm ligands remaining on the PQD surface. [Figure 3D](#) presents the incident photon-to-electron conversion efficiency (IPCE) spectra of PQDSCs, and the 2-PeOH/Cl-based PQDSC shows relatively higher IPCE values than that of the EtOAc/Cl-based device, resulting in a higher  $J_{SC}$  in 2-PeOH/Cl-based PQDSC. [Figure 3E](#) shows the stabilized power output (SPO) of the 2-PeOH/Cl-based PQDSC for which a stabilized PCE of ~15.68% was obtained; this is much higher than that of the EtOAc/Cl-based PQDSC with a stabilized PCE of 13.90% ([Figure S16](#)).

We collected 20 cells fabricated from different batches to study the reproducibility. [Figure 3F](#) shows the statistical photovoltaic parameters of EtOAc/Cl and 2-PeOH/Cl-based PQDSCs. It can be seen that these PQDSCs are highly reproducible. In comparison with an average PCE of 14.46%  $\pm$  0.4% for EtOAc/Cl-based devices, 2-PeOH/Cl-based PQDSCs demonstrate a higher average PCE of 16.13%  $\pm$  0.4%. Additionally, the performance of PQDSCs fabricated with Cl ligands in other alcohols was also counted in statistics ([Figure S17](#)), and the variation trend of photovoltaic performance is almost identical to that of the PQDSCs fabricated with the corresponding neat solvents ([Figure 1B](#)), indicating that the solvent plays a decisive role during the post-treatment of PQD solid films.

Although a suitable solvent of short ligands for the post-treatment of PQD solid film could promote the removal of long-chain insulating ligands from the PQD surface and thereby improve the performance of PQDSCs, the removal of pristine OA/OAm ligands may inevitably introduce vacancies on the PQD surface. Molecules around these vacancies show high activity and diffusivity, therefore resulting in that PQDs are susceptible to moisture and oxygen attacking.<sup>56,59</sup> 2-PeOH-based PQDs have partially changed into the  $\delta$ -phase after aging for 10 days under an RH of 25%–35%, whereas 2-PeOH/Cl-based PQDs show no morphological and phase transition after aging ([Figures S18A](#) and [S18B](#)). Meanwhile, the PL intensity of PQDs with 2-PeOH/Cl post-treatment was also improved compared with that of the PQDs with neat 2-PeOH post-treatment ([Figure S18C](#)), indicating that the Cl ligands could effectively suppress the nonradiative recombination by passivating the surface defects of PQDs. Therefore, Cl ligands could substantially improve the stability of PQD solid films by filling the vacancies on the PQD surface and thus diminishing the attacking sites of moisture and oxygen.

The improved stability of PQD solid films may in turn improve the shelf life of PQDSCs. Therefore, the stabilities of unencapsulated 2-PeOH and 2-PeOH/Cl-based PQDSCs

were tested.<sup>60</sup> The PQDSCs were stored under dry air condition with an RH of 5%–15%. Figure 3G shows the evolution of the normalized PCE along with the aging time, and the corresponding pristine J-V curves are summarized in Figure S19. It can be seen that after aging for 960 h, 2-PeOH-based PQDSC only maintains ~45% of its initial PCE, whereas 2-PeOH/Cl-based PQDSC retains ~93% of its initial PCE. Moreover, the stability of un-encapsulated pristine and EtOAc/Cl-based PQDSCs was also tested, which shows that ~51% and ~80% of the initial efficiencies of pristine and EtOAc/Cl-based PQDSCs are retained, respectively, after aging for 960 h under dry air condition (Figure S20). The operational stability of PQDSCs was also measured under continuous 100 mW cm<sup>-2</sup> illumination for 100 h. As shown in Figure 3H, after using Cl ligands to passivate the PQD surface, the photostability of PQDSCs is significantly improved such that ~80% of its initial PCE is maintained in 2-PeOH/Cl-based PQDSC, whereas only ~30% of its initial PCE can be retained in the 2-PeOH-based PQDSC. The improved operational stability of PQDSCs is ascribed to the suppressed vacancy-mediated ion migration under continuous illumination after passivating the surface vacancies of PQDs using Cl ligands, since ion migration has been reported to be one of the decisive reasons for the performance degradation of PSCs.<sup>61,62</sup> These important results confirm that ligand engineering of PQDs is critical to improve the photovoltaic performance and device stability of PQDSCs.

### Charge carrier collection and recombination

To fundamentally understand the causes of improved performance in 2-PeOH/Cl-based PQDSCs, the charge carrier dynamics within the PQDSCs were investigated in depth. Confocal PL mapping was measured to observe *in situ* the PL emission distribution of PQD solid films. As shown in Figures 4A and 4B, 2-PeOH/Cl-based PQD solid film shows a more homogeneous PL emission distribution than the EtOAc/Cl-based sample, suggesting that the charge carrier recombination within the PQD solid film is more balanced after the 2-PeOH/Cl post-treatment. Meanwhile, the 2-PeOH/Cl-based PQDs exhibit a stronger PL emission intensity and longer PL lifetime than EtOAc/Cl-based PQDs (Figures 4C and S21; Table S5). These results indicate that the nonradiative recombination within the 2-PeOH/Cl-based PQD solid film is further suppressed, resulting from the more uniform and complete surface passivation of PQDs mediated with 2-PeOH.

The trap densities within the PQD solid films were quantitatively investigated by conducting SCLC tests on the electron-only devices (Figure 4D), which shows that the EtOAc/Cl-based PQD solid film has a  $V_{TF}$  of ~0.23 V, corresponding to a  $N_{trap}$  of  $\sim 0.64 \times 10^{15} \text{ cm}^{-3}$ , whereas the  $V_{TF}$  and  $N_{trap}$  of the 2-PeOH/Cl-based PQD solid film are decreased to ~0.18 V and  $\sim 0.5 \times 10^{15} \text{ cm}^{-3}$ . The calculated  $\mu_e$  was also increased in the 2-PeOH/Cl-based PQD solid film ( $1.98 \times 10^{-3} \text{ cm}^2 \text{ V}^{-1} \text{ s}^{-1}$ ) in comparison with the EtOAc/Cl-based PQD solid film ( $3.85 \times 10^{-4} \text{ cm}^2 \text{ V}^{-1} \text{ s}^{-1}$ ). This indicates that Cl could better passivate the PQD surface under the mediation of 2-PeOH solvent and did not affect the charge carrier transport within the PQD solid film due to its better conductivity than insulating OAm ligands. Transient photovoltage (TPV) and transient photocurrent (TPC) techniques could offer more insights into the charge carrier recombination within the PQDSCs. Figure 4E shows the TPV curves of PQDSCs, and the decay curves were fitted using a bi-exponential function. A longer charge carrier lifetime (slower charge carrier recombination rate) within a solar cell generally indicates less charge carrier recombination. As expected, the 2-PeOH/Cl-based PQDSC shows a substantially prolonged charge carrier lifetime of 2.59 ms compared with that of 1.59 ms in the EtOAc/Cl-based PQDSC. The TPC profiles were fitted using a single exponential function (Figure 4F). The decay time in the 2-PeOH/Cl-based PQDSC (1.44 μs) was also decreased compared

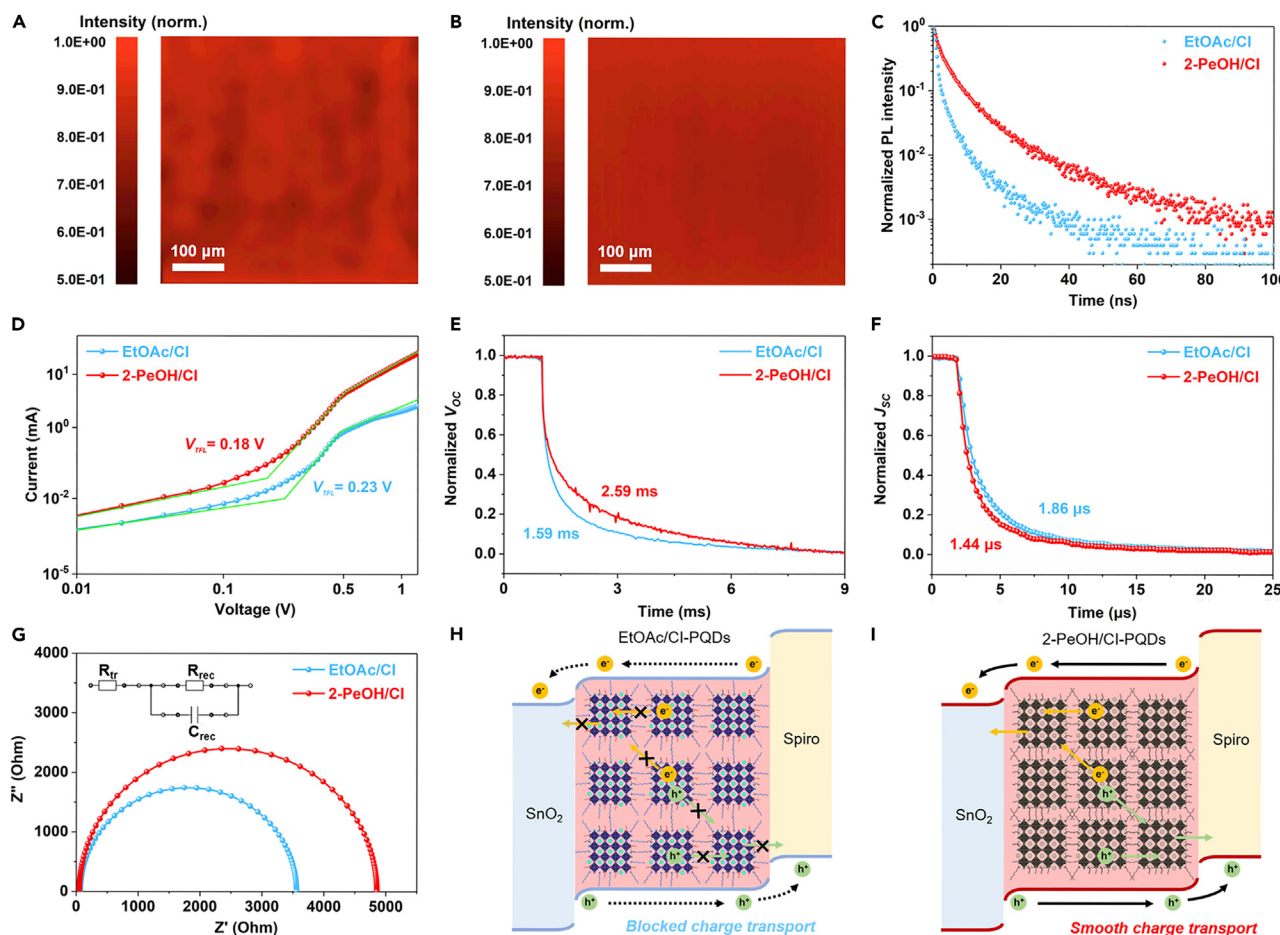


**Figure 4. Charge carrier collection and recombination**

(A and B) Normalized confocal PL mapping images of EtOAc/Cl-based PQD solid film (A) and 2-PeOH/Cl-based PQD solid film (B).

(C and D) TRPL spectra (C) and SCLC curves (D) of EtOAc/Cl and 2-PeOH/Cl-based PQD solid films.

(E–G) Normalized TPV curves (E), normalized TPC curves (F), and EIS curves (G) of EtOAc/Cl and 2-PeOH/Cl-based PQDSCs.

(H and I) Schematic illustration of charge carrier collection and recombination within the EtOAc/Cl-based PQDSC (H) and 2-PeOH/Cl-based PQDSC (I).

with that in the EtOAc/Cl-based PQDSC ( $1.86 \mu\text{s}$ ), demonstrating a better charge carrier extraction of the 2-PeOH/Cl-based PQDSC.

The light intensity-dependent  $V_{OC}$  and  $J_{SC}$  of PQDSCs were further studied to obtain more details concerning the charge carrier behaviors. The  $V_{OC}$  as a function of light intensity is expressed as  $nkT/q$ , where  $n$ ,  $k$ ,  $T$ , and  $q$  are the diode ideality factor, Boltzmann constant, Kelvin temperature, and elementary charge, respectively.<sup>63</sup> The diode ideality factor was calculated to be 1.46 for the 2-PeOH/Cl-based PQDSC, lower than that of 1.84 for the EtOAc/Cl-based device (Figure S22A). The smaller diode ideality factor of the 2-PeOH/Cl-based PQDSC indicates alleviated trap-assisted charge carrier recombination in solar cells. The incident light intensity-dependent  $J_{SC}$  generally follows the relationship of  $J_{SC} \propto I^\alpha$ , where  $I$  and  $\alpha$  are the incident light intensity and exponential factor, respectively. The  $\alpha$  value closer to 1 generally suggests that the competition between charge carrier recombination and collection is less affected by the light intensity.<sup>64</sup> The  $\alpha$  values were fitted to be 0.98 and 0.99 for EtOAc/Cl and 2-PeOH/Cl-based PQDSCs (Figure S22B), respectively, revealing that both solar cells appear close to linear photocurrent with light intensity. Meanwhile, the 2-PeOH/Cl-based PQDSC exhibits a lower current

leakage, compared with the EtOAc/Cl-based device, further confirming suppressed charge carrier recombination within the 2-PeOH/Cl-based PQDSC ([Figure S22C](#)).

Electrochemical impedance spectroscopy (EIS) was further measured to examine the charge carrier transport within the PQDSCs. [Figure 4G](#) shows the Nyquist plots and the equivalent circuit model of EtOAc/Cl and 2-PeOH/Cl-based PQDSCs; the profile at the low-frequency region demonstrates the recombination chemical capacitance ( $C_{rec}$ ) and recombination resistance ( $R_{rec}$ ) of devices, and the profile at the high-frequency region generally demonstrates the charge transport resistance ( $R_{tr}$ ). The 2-PeOH/Cl-based PQDSC possesses a smaller  $R_{tr}$  of 50.2 Ω and larger  $R_{rec}$  of 4,810 Ω in comparison with the  $R_{tr}$  of 67.4 Ω and  $R_{rec}$  of 3,490 Ω for the EtOAc/Cl-based PQDSC, suggesting that the charge carrier recombination and transport within the device are effectively suppressed and facilitated, respectively. These results are in good agreement with the above optoelectronic properties of PQDs and the photovoltaic performance of PQDSCs, confirming that the long-chain OAm ligands can be more substituted with short Cl ligands under the mediation of 2-PeOH.

Based on these results, we proposed a model to fundamentally understand the causes of the improved performance in 2-PeOH/Cl-based PQDSCs. When the conventional aprotic EtOAc with a lower dielectric constant is used as the solvent for ligand exchange during the post-treatment of PQD solid films, pristine insulating OAm ligands on the PQD surface could be not sufficiently removed and subsequently substituted by short ones, resulting in unsatisfactory surface defect passivation of PQDs. Therefore, after the conventional ligand exchange within EtOAc, massive long-chain insulating ligands remain on the PQD surface that significantly affect the charge carrier transport within the PQD solid films, which can be verified by the lower FF in EtOAc/Cl-based PQDSCs ([Figure 4H](#)). However, when the protic 2-PeOH with an appropriate dielectric constant and acidity is applied as the solvent for ligand exchange during the post-treatment of PQD solid films, the pristine insulating OAm ligands on the PQD surface can be more sufficiently removed without introducing halogen vacancy defects on the PQD surface, leading to better charge carrier transport within the PQD solid films. Meanwhile, the high solubility of Cl ligands in 2-PeOH allows for efficient passivating surface defects of PQDs, lowering the nonradiative recombination. Therefore, taking advantage of good charge carrier transport within the PQD solid films and efficient surface defect passivation of PQDs, the charge carrier recombination is substantially diminished in the 2-PeOH/Cl-based PQDSCs, resulting in the increased FF and consequently improving the photovoltaic performance and stability of devices ([Figure 4I](#)).

### Theoretical calculations

First-principles density functional theory (DFT) calculations were carried out to obtain more details concerning the solvent-mediated ligand exchange and its effect on the surface properties of PQDs, and the detailed calculation method is described in the [Note S3](#). The interaction of OAm cation with EtOAc or 2-PeOH was first studied. The main interaction force is the hydrogen bond formed by the interaction of the N–H bond of the OAm proton donor and the oxygen atom of the solvent proton acceptor.<sup>65</sup> Typically, we chose one of three N–H bonds of an OAm cation as the main research object, which was combined with EtOAc or 2-PeOH to calculate the interaction energy ( $E_{interaction}$ ). For the monosolvated system ([Figures 5A and 5B](#)), the  $E_{interaction}$  of OAm with EtOAc (OAm prefers to interact with the double-bonded O atom of EtOAc, and another suboptimal case is shown in [Figure S23A](#)) is slightly higher than that of OAm with 2-PeOH, which is due to the increased electron density of the double-bonded O atom caused by the P–π conjugation of the ester group

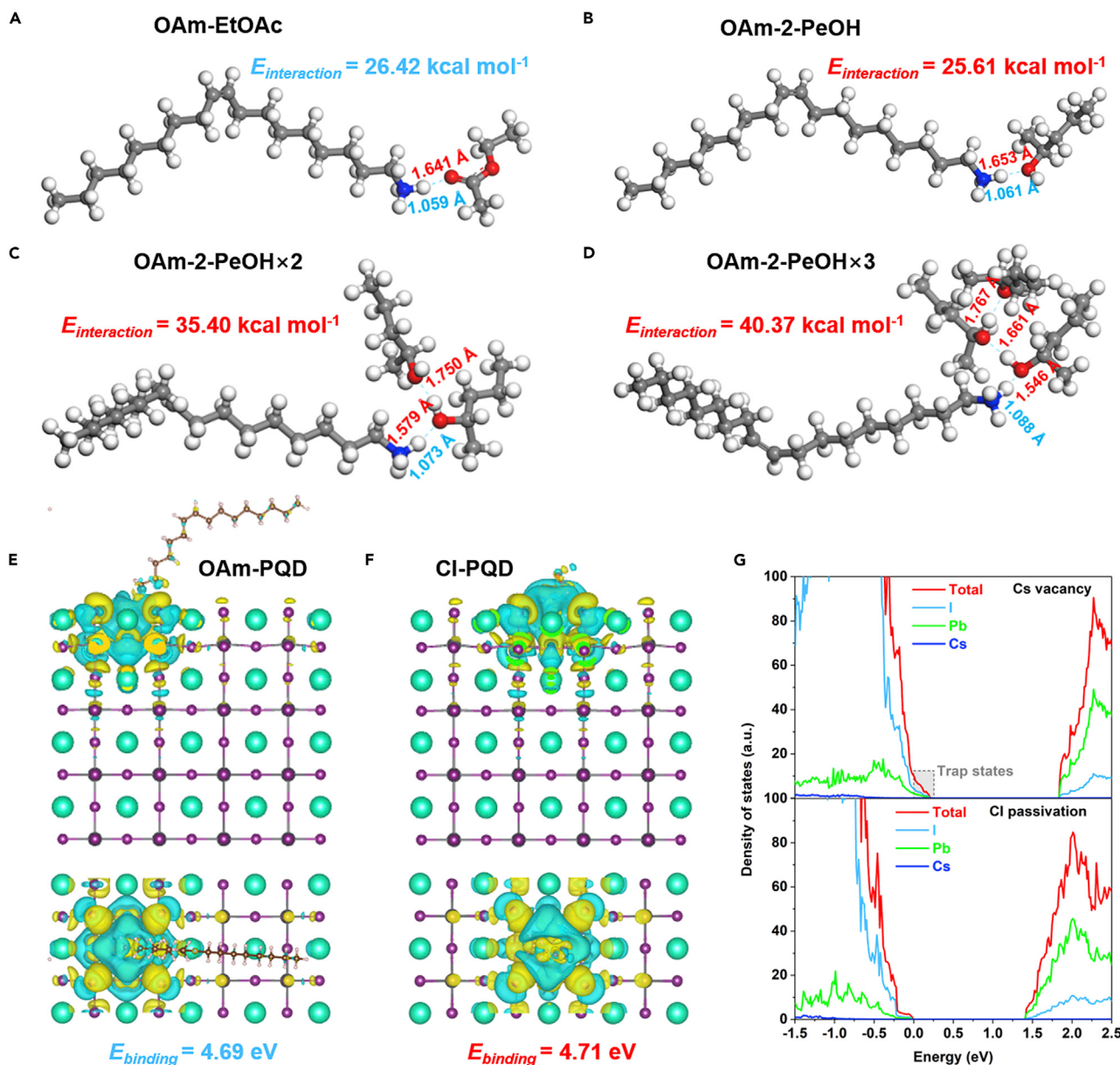


**Figure 5. Theoretical calculations**

(A-D) Equilibrium geometries of OAm-EtOAc (A), OAm-2-PeOH (B), OAm-2-PeOH  $\times$  2 (C), and OAm-2-PeOH  $\times$  3 (D) systems, and the models were optimized at the B3LYP-D3 (BJ)/6-31+G\* level. Bond lengths ( $\text{\AA}$ ) of hydrogen bonds ( $\text{N}-\text{H}\cdots\text{O}$ ) were also calculated.

(E and F) Differential charge density plots of OAm (E) and Cl (F) ligands bind to the  $\text{CsPbI}_3$  PQD {001} surface. The isosurface level of the differential charge densities is 0.002 electrons Bohr $^{-3}$ , and the yellow and blue regions represent the accumulation and depletion of electrons, respectively.

(G) DOS curves of the PQD surface with an A-site vacancy (upper) and passivated by a Cl ligand (bottom).

within the EtOAc molecule, as shown in the electrostatic potential plots in Figures S23B–S23E. However, due to the  $E_{interaction}$  between aprotic EtOAc molecules being negligibly weak, further reaction hardly occurs between the EtOAc and OAm. By contrast, the O atom of protic 2-PeOH molecules could continuously increase its electron density through the continuous formation of intermolecular hydrogen bonds. As shown in Figures 5C and 5D, with the number of 2-PeOH molecules simultaneously binding to OAm cation increases,  $E_{interaction}$  gradually increases. In particular, when OAm and 2-PeOH form a trihydrated system, the

$E_{interaction}$  of OAm with 2-PeOH (40.37 kcal mol<sup>-1</sup>) is ~1.5 times higher than that of the OAm with EtOAc (26.42 kcal mol<sup>-1</sup>), which corresponds to the decrease in length of the O···H hydrogen bond from 1.641 to 1.546 Å. In the practical solvent environment, more N–H bonds could interact with more solvent molecules and their difference in  $E_{interaction}$  further increased, resulting in 2-PeOH dissociating more OAm ligands from the PQD surface. Furthermore, the slight difference in the acidity coefficients ( $pK_a$ ) of EtOH (15.9) and 1-BuOH (16.1) antisolvents would also result in a great distinction in the contents of the resultant QD surface carboxyl ligands.<sup>28</sup> The Gibbs free energy changes for dissociating a proton ( $\Delta G_{aq}$ ) of 1-PeOH or 2-PeOH were also calculated to evaluate its ability to remove acetate ligands from the PQD surface, and the results are summarized in Table S9.<sup>66</sup> It can be observed that the calculated  $\Delta G_{aq}$  of 1-PeOH is smaller than that of 2-PeOH, indicating that it is more liable for 1-PeOH to dissociate protons, thereby attacking and dissolving the acetate ligands on the PQD surface.

To study the passivation effect of Cl ligands on the surface properties of PQDs, we constructed models of pristine OAm and Cl ligands anchored on the {001} lattice plane of CsI-terminated PQDs with an A-site (Cs) vacancy, and the corresponding differential charge density plots are displayed in Figures 5E and 5F. The binding energies ( $E_{binding}$ ) of OAm and Cl ligands on the PQD surface are calculated to be similar, which are 4.69 and 4.71 eV, respectively. Therefore, the ligand exchange of OAm with Cl ligands may be not in a conventional manner that only depends on different binding energies of ligands. Meanwhile, the amount of the pristine OAm ligands removed by the solvent determines the completeness of ligand exchange. Bader charge analysis was further performed to quantify the electron transfer, and there is an extremely small charge transfer of 0.04 e<sup>-</sup> between the Cl ligand and PQD surface, indicating that the Cl ligand could only passivate surface A-site vacancy without changing the chemical nature of PQD surface.<sup>57</sup> In addition, the electronic structures of PQDs were further calculated to study the ligand passivation effect. The upper figure of Figure 5G shows the density of state (DOS) of PQDs with an A-site vacancy in which the shallow-level defects exist within the band gap. These shallow-level defects could act as nonradiative recombination centers, which are unfavorable for the optoelectronic properties of PQDs and the photovoltaic performance of PQDSCs. However, after passivating the A-site vacancy with the Cl ligand, the detrimental trap states are thoroughly diminished (Figure 5G, bottom). These theoretical calculation results are consistent with the above experimental results, revealing that tailoring the ligand exchange mediated by an appropriate solvent can substantially improve the surface properties of PQDs and thus the photovoltaic performance of PQDSCs.

In addition to Cl ligands, the versatility of other ligands applied to substitute the pristine OAm ligands on the PQD surface under the mediation of 2-PeOH was further studied. The conventional short ligands, such as GAI,<sup>16</sup> PEAI,<sup>24</sup> FAI,<sup>23</sup> and DMAI,<sup>45</sup> were dissolved in the 2-PeOH for the post-treatment of PQD solid films. For comparison, these ligands were also dissolved in the conventional EtOAc for the post-treatment of PQD solid films. The light absorption and steady-state PL spectra of PQD solid films, as well as the J-V curves of the corresponding PQDSCs, are shown in Figure S24. As expected, the PQD solid films and PQDSCs fabricated based on the solvent-mediated ligand exchange show improved performance compared with those fabricated based on the conventional ligand exchange (the details about the performance characterization are presented in Note S4), which demonstrates a universality and feasible ligand exchange platform provided by using 2-PeOH as the solvent for the ligand exchange of PQDs.

Based on the above results of the ligand exchange of PQDs and the device performance of PQDSCs, the following criteria may need to be taken into account when selecting the solvents for the post-treatment of PQD solid films: (1) the solvent with good ligand solubility could provide sufficient ligand sources to improve the ligand exchange of PQDs, thus diminishing charge carrier recombination within the PQDSCs; (2) a suitable dielectric constant could ensure proper electrostatic interactions between the charged surface ligands and solvent, thereby achieving a stable PQD surface state that is favorable for charge carrier transport within PQD solid films; (3) protic type could ensure a high solubility of ionic salt ligands that can be used to regulate the PQD surface ligands by forming hydrogen bonds between the ligand and solvent; and (4) HBD acidity could specifically evaluate the ability of a solvent to dissociate the short carboxyl ligands on the PQD surface by providing protons. Notably, these factors are of equal importance for the ligand exchange PQDs during the post-treatment of PQD solid films, and consequently, 2-PeOH was preferably selected as the solvent for the post-treatment of CsPbI<sub>3</sub> PQD solid films. We believe that these criteria could be also applied to the PQD systems with various components—whose surface is dual terminated with OA/OAm ligands—such as FA-containing PQDs, thereby realizing the next milestone in the photovoltaic performance of PQDSCs.

## Conclusions

In summary, an efficient solvent-mediated ligand exchange of PQDs was demonstrated to achieve a better ligand substitution for high-performing solar cells. Considering the dielectric constant and acidity, 2-PeOH was screened as an ideal solvent of short ligands for the post-treatment of PQD solid films to sufficiently remove pristine insulating OAm ligands from the PQD surface without introducing halogen vacancy defects, thereby improving the charge carrier transport within the PQD solid films. Additionally, the good solubility of short ligands in the protic 2-PeOH allowed for efficient surface defect passivation of PQDs, thus significantly diminishing nonradiative recombination and improving the stability of PQD solid films. As a result, by using the 2-PeOH as the solvent and Cl as the short ligand for the post-treatment of PQD solid films, the PQDSC yielded a PCE of 16.53%, which is the highest value obtained among inorganic PQDSCs. The high photovoltaic performance of 2-PeOH/Cl-based PQDSCs was attributed to the significantly improved charge carrier collection and substantially diminished charge carrier recombination of PQDSCs. Moreover, the stability of PQDSC was also improved through efficiently passivating surface defects of PQDs using Cl ligands. This work provides a universal and feasible ligand exchange platform to regulate the surface ligand chemistry of PQDs for realizing high-performing solar cells or other optoelectronic devices.

## EXPERIMENTAL PROCEDURES

### Resource availability

#### Lead contact

Further information and requests for resources and materials should be directed to and will be fulfilled by the lead contact, Xiaoliang Zhang ([xiaoliang.zhang@buaa.edu.cn](mailto:xiaoliang.zhang@buaa.edu.cn))

#### Materials availability

This study did not generate new unique materials.

### Data and code availability

This study did not generate or analyze datasets or code. The data employed to support the current study are available from the [lead contact](#) upon reasonable request.

### Materials

All reagents were used as received without further purification. 1-Octadecene (ODE, >90.0% [GC]), cesium carbonate (Cs<sub>2</sub>CO<sub>3</sub>, 99.99% metals basis), OA (technical grade 90%), OAm (technical grade 80%–90%), MeOAc (anhydrous 99.5%), EtOAc (spectrographic grade 99.5%), n-hexane (>99% [GC]), n-octane (>99% [GC]), EtOH ( $\geq$  99.5%), and MeOH (99%) were purchased from Aladdin. t-PeOH (99%), 2-PeOH (99%), 1-PeOH (ACS, 99+%), t-BuOH (99%), 1-BuOH (anhydrous, 99.9%), chlorobenzene (CB, anhydrous, 99.8%) and SnO<sub>2</sub> (15% in H<sub>2</sub>O colloidal dispersion) were purchased from Alfa Aesar. FAI ( $\geq$  99.5%), dimethylammonium iodide (DMAI,  $\geq$  99.5%), phenethylammonium iodide (PEAI,  $\geq$  99.5%), PbI<sub>2</sub> (99%), 2,2',7,7'-tetrakis (N,N-di-p-methoxyphenylamine)-9,9'spirobifluorene (spiro-O-MeTAD,  $\geq$  99.5%) and tris(2-(1H-pyrazol-1-yl)-4-tert-butylpyridine)-cobalt(III)Tris(bis(trifluoromethylsulfonyl)imide)) (FK 209) were purchased from Xi'an Polymer Light Technology. i-PrOH (99.5%), 4-tert-butylpyridine (4-TBP, 96%), lithium bis(trifluoromethylsulfonyl)imide (Li-TFSI), and acetonitrile (anhydrous, 99.8%) were purchased from Sigma-Aldrich. Cl (98%) and guanidinium iodide (GAI, 97%) were purchased from TCI.

### PQD solid film preparation

Each layer of CsPbI<sub>3</sub> PQDs was spin-coated using a PQD solution (~85 mg/mL in octane) at the speed of 1,000 RPM for 10 s and 2,000 RPM for 20 s (the details about the synthesis and purification of CsPbI<sub>3</sub> PQDs are summarized in [Note S5](#)). Neat MeOAc antisolvent was then pipetted onto the film and kept for 5 s and then dried by spinning at 2,000 RPM for 30 s. The PQD solid film was subsequently rinsed again with MeOAc for 2 s and spin-dried at 2,000 RPM for 30 s. The above procedure was repeated 2–5 times to obtain a film with a thickness of 200–600 nm. The neat EtOAc and alcohols (t-PeOH, 2-PeOH, 1-PeOH, t-BuOH, 1-BuOH, i-PrOH, EtOH, and MeOH), or the EtOAc and alcohol solutions of ligands were loaded onto the assembled PQD solid film for 5 s and spun at 2,000 RPM for 60 s, followed by rinsing the film with EtOAc for 2 s and spin-dried at 2,000 RPM for 30 s. The ligand solutions were obtained by dissolving ligands (Cl, GAI, PEAI, DMAI and FAI) in EtOAc and alcohols with desirable concentrations (Cl, GAI and PEAI for 0.1 mg mL<sup>-1</sup>, DMAI and FAI for 0.05 mg mL<sup>-1</sup>), followed by ultra-sonicating for 30 min. It should be noted that, compared with the high solubility of the aforementioned ionic salts in protic alcohols, the solubility of these ligands in aprotic EtOAc was very limited and difficult to accurately control. In particular, Cl was still saturated in EtOAc with a concentration as low as 0.05 mg mL<sup>-1</sup>, thus the undissolved salts needed to be removed by centrifugation at 4,000 RPM for 3 min.

### Material characterization

XRD pattern was measured using a diffractometer (D/MAX-2500, Rigaku) with Cu K $\alpha$  radiation ( $\lambda = 1.54 \text{ \AA}$ ). The scanning range of the diffraction angle was from 5° to 50°. FTIR was carried out using the Nicolet 6700 FTIR Spectrometer in the transmittance mode. The light absorption spectrum was measured using a UV-vis spectrophotometer (Maya2000 Pro, Ocean Optical). Steady-state PL spectra were recorded through a spectrofluorometer with an excitation of 490 nm (LLS-490, Ocean Optical). PL mapping images were captured by an optic spectrometer (NOVA, Ideaoptics Technology) with an automatically controlled microscopic platform. TRPL decay spectra were tested using a picosecond diode laser (FLS980) with an excitation light of 470 nm and a cutoff filter (570 nm) was used to avoid the scattered excitation light

during the measurement. The morphology of PQDs was characterized using a transmission electron microscope (JEM-2100, JEOL) at an accelerating voltage of 200 kV. XPS measurement was performed using the Thermo ESCALAB 250Xi ultraviolet photoelectron spectrometer with a He I (21.22 eV) UV-light source as the excitation source.

### Solar cell fabrication

The ITO glass substrate was sonicated in order of acetone, deionized water, and ethanol for 30 min. The washed substrates were dried and treated with ultraviolet ozone for 20 min to improve surface wettability and remove ionic and organic contaminants. The SnO<sub>2</sub> nanoparticle solution (2.67%, diluted with deionized water) was spin-coated on the ITO substrate at 4,000 RPM for 30 s and annealed at 150°C for 30 min. The PQD solid film was deposited using the procedure described above, resulting in a suitable thickness of ~550 nm. Afterward, Spiro-OMeTAD solution was spin-coated on the top of PQD solid film at 4,000 RPM for 30 s. The spiro-OMeTAD solution was prepared by dissolving Spiro-OMeTAD in CB with a concentration of 72.3 mg/mL, then added with 28.8 μL of 4-TBP, 17.5 μL of Li-TFSI solution in acetonitrile (520 mg/mL), and 10 μL of FK 209 solution in acetonitrile (300 mg/mL). All the spin-coating procedures were carried out under ambient conditions in which the deposition of PQD solid films and Spiro-OMeTAD were carried out under the conditions of 20%–30% RH and <20% RH, respectively. Finally, the PQDSCs were completed after thermally evaporating the Ag electrode with a thickness of ~100 nm.

### Solar cell characterization

The current density-voltage (J-V) curve of devices was measured under one sun illumination (AM 1.5G, 100 mW cm<sup>-2</sup>) provided by a solar simulator (Enli Technology SS-F5-3A) and recorded using the Keithley 2400 digital source meter. The device was tested in an N<sub>2</sub> atmosphere. The working area was 4 mm<sup>2</sup> defined using a black metallic mask. Before testing, the light intensity was calibrated using a certified reference silicon solar cell (SRC-2020, Enlitech). The voltage sweep rate was 20 mV with a delay of 20 ms for the reverse (forward) sweeping direction from 1.4 (−0.2 V) to −0.2 V (1.4 V). A slight steepness of the measured J-V curves may be caused by the charge carriers needing to pass through more interfaces during transport in the PQDSCs. The IPCE spectra of devices were obtained by an Enli Technology QE-R system. The setup was calibrated using a certified reference silicon solar cell (SRC-2020, Enlitech) before the measurement. For the SPO measurement, the device was measured by holding the device at the maximum power point and monitoring the photocurrent variation under AM 1.5G illumination. The device photostability was measured using the solar cell stability test setup (PV-S-16, Tianjin Meitong, China) in an N<sub>2</sub> atmosphere, which was conducted under continuous 100 mW/cm<sup>2</sup> illumination provided by a white LED (MT-LED-80, Tianjin Meitong, China), and the results were automatically recorded by the aging test software. TPV, TPC, and electrochemical impedance spectroscopy (EIS) were recorded by a composite electrochemical workstation (Zahner Zennium CIMPS-pro), which could obtain the time constants relating to the charge carrier recombination in the device.

The SCLC measurement was performed in dark conditions using Keithley 2400 to record the I-V curve of the electron-only device fabricated with the structure of ITO/SnO<sub>2</sub>/PQDs/PCBM/Ag. The trap density ( $N_{\text{trap}}$ ) of PQD solid film was calculated using the following equation:

$$N_{\text{trap}} = \frac{2\epsilon_0\epsilon_r V_{\text{TFL}}}{eL^2} \quad (\text{Equation 2})$$

where  $V_{TFL}$ ,  $L$ ,  $\epsilon_0$ ,  $\epsilon_r$ , and  $e$  are the trap-filled limit voltage, film thickness, vacuum permittivity, relative dielectric constant, and elementary charge, respectively. The  $V_{TFL}$  was determined by the intersection of the tangent lines between the ohmic and the trap-filling zone (the first inflection point in the  $I$ - $V$  curve). The electron mobility ( $\mu_e$ ) PQD solid film was calculated using the following equation:

$$\mu_e = \frac{8J_DL^3}{9\epsilon_0\epsilon_rV^2} \quad (\text{Equation 3})$$

where  $J_D$ ,  $V$ , and  $L$  are the dark current density measured in the high voltage SCLC regime, applied voltage, and film thickness, respectively.

## SUPPLEMENTAL INFORMATION

Supplemental information can be found online at <https://doi.org/10.1016/j.joule.2022.05.007>.

## ACKNOWLEDGMENTS

This work was supported by the National Natural Science Foundation of China (grant no. 51872014), the Recruitment Program of Global Experts, Fundamental Research Funds for the Central Universities, and the "111" Project (B17002). This work was also supported by the HPC of Beihang University.

## AUTHOR CONTRIBUTIONS

X. Z. and D.J. designed the research and experiments. D.J. and J.C. synthesized PQDs; conducted XRD measurement; measured FTIR spectra, light absorption, and PL spectra; and measured/analyzed SEM images. D.J. fabricated solar cells and measured the solar cell performance. D.J. and J.Q. conducted DFT calculations with the help of H.M. D.J. wrote the first version of the manuscript and prepared the figures. All authors contributed to discussions and commented on the manuscript, and all authors reviewed the manuscript.

## DECLARATION OF INTERESTS

The authors declare no competing interests.

Received: October 13, 2021

Revised: January 28, 2022

Accepted: May 11, 2022

Published: June 6, 2022

## REFERENCES

1. Protesescu, L., Yakunin, S., Bodnarchuk, M.I., Krieg, F., Caputo, R., Hendon, C.H., Yang, R.X., Walsh, A., and Kovalenko, M.V. (2015). Nanocrystals of cesium lead halide perovskites (CsPbX<sub>3</sub>, X = Cl, Br, and I): novel optoelectronic materials showing bright emission with wide color gamut. *Nano Lett.* 15, 3692–3696.
2. Chen, J., Jia, D., Johansson, E.M.J., Hagfeldt, A., and Zhang, X. (2021). Emerging perovskite quantum dot solar cells: feasible approaches to boost performance. *Energy Environ. Sci.* 14, 224–261.
3. Kovalenko, M.V., Protesescu, L., and Bodnarchuk, M.I. (2017). Properties and potential optoelectronic applications of lead halide perovskite nanocrystals. *Science* 358, 745–750.
4. Yang, H., Gutiérrez-Arzaluz, L., Maity, P., Abdulhamid, M.A., Yin, J., Zhou, Y., Chen, C., Han, Y., Szekely, G., Bakr, O.M., and Mohammed, O.F. (2021). Air-resistant lead halide perovskite nanocrystals embedded into polyimide of intrinsic microporosity. *Energy Mater. Adv.* 2021, 1–9.
5. Mei, X., Jia, D., Chen, J., Zheng, S., and Zhang, X. (2022). Approaching high-performance light-emitting devices upon perovskite quantum dots: advances and prospects. *Nano Today* 43, 101449.
6. Yakunin, S., Protesescu, L., Krieg, F., Bodnarchuk, M.I., Nedelcu, G., Humer, M., De Luca, G., Fiebig, M., Heiss, W., and Kovalenko, M.V. (2015). Low-threshold amplified spontaneous emission and lasing from colloidal nanocrystals of caesium lead halide perovskites. *Nat. Commun.* 6, 8056.
7. Shen, K., Xu, H., Li, X., Guo, J., Sathasivam, S., Wang, M., Ren, A., Choy, K.L., Parkin, I.P., Guo, Z., and Wu, J. (2020). Flexible and self-powered photodetector arrays based on all-inorganic CsPbBr<sub>3</sub> quantum dots. *Adv. Mater.* 32, e2000004.
8. Zheng, C., Liu, A., Bi, C., and Tian, J. (2020). SCN-doped CsPbI<sub>3</sub> for improving stability and photodetection performance of colloidal quantum dots. *Acta Phys. Chim. Sin.* 37, 2007084.
9. Jia, D., Chen, J., Yu, M., Liu, J., Johansson, E.M.J., Hagfeldt, A., and Zhang, X. (2020). Dual passivation of CsPbI<sub>3</sub> perovskite nanocrystals

- with amino acid ligands for efficient quantum dot solar cells. *Small* 16, e2001772.
10. Jia, D., Chen, J., Mei, X., Fan, W., Luo, S., Yu, M., Liu, J., and Zhang, X. (2021). Surface matrix curing of inorganic CsPbI<sub>3</sub> perovskite quantum dots for solar cells with efficiency over 16%. *Energy Environ. Sci.* 14, 4599–4609.
  11. Duan, L.P., Hu, L., Guan, X.W., Lin, C.H., Chu, D.W., Huang, S.J., Liu, X.G., Yuan, J.Y., and Wu, T. (2021). Quantum dots for photovoltaics: A tale of two materials. *Adv. Energy Mater.* 11, 2100354.
  12. Swarnkar, A., Marshall, A.R., Sanehira, E.M., Chernomordik, B.D., Moore, D.T., Christians, J.A., Chakrabarti, T., and Luther, J.M. (2016). Quantum dot-induced phase stabilization of  $\alpha$ -CsPbI<sub>3</sub> perovskite for high-efficiency photovoltaics. *Science* 354, 92–95.
  13. Zhao, Q., Hazarika, A., Schelhas, L.T., Liu, J., Gaulding, E.A., Li, G., Zhang, M., Toney, M.F., Sercel, P.C., and Luther, J.M. (2019). Size-dependent lattice structure and confinement properties in CsPbI<sub>3</sub> perovskite nanocrystals: negative surface energy for stabilization. *ACS Energy Lett.* 5, 238–247.
  14. Zhao, Q., Hazarika, A., Chen, X., Harvey, S.P., Larson, B.W., Teeter, G.R., Liu, J., Song, T., Xiao, C., Shaw, L., et al. (2019). High efficiency perovskite quantum dot solar cells with charge separating heterostructure. *Nat. Commun.* 10, 2842.
  15. Hao, M., Bai, Y., Zeiske, S., Ren, L., Liu, J., Yuan, Y., Zarrabi, N., Cheng, N., Ghasemi, M., Chen, P., et al. (2020). Ligand-assisted cation-exchange engineering for high-efficiency colloidal Cs<sub>1-x</sub>FA<sub>x</sub>PbI<sub>3</sub> quantum dot solar cells with reduced phase segregation. *Nat. Energy* 5, 79–88.
  16. Ling, X., Yuan, J., Zhang, X., Qian, Y., Zakeeruddin, S.M., Larson, B.W., Zhao, Q., Shi, J., Yang, J., Ji, K., et al. (2020). Guanidinium-assisted surface matrix engineering for highly efficient perovskite quantum dot photovoltaics. *Adv. Mater.* 32, e2001906.
  17. Chen, J., Jia, D., Qiu, J., Zhuang, R., Hua, Y., and Zhang, X. (2022). Multideterminate passivation crosslinking perovskite quantum dots for efficient solar cells. *Nano Energy* 96, 107140.
  18. Lim, S., Lee, G., Han, S., Kim, J., Yun, S., Lim, J., Pu, Y.-J., Ko, M.J., Park, T., Choi, J., and Kim, Y. (2021). Monodisperse perovskite colloidal quantum dots enable high-efficiency photovoltaics. *ACS Energy Lett.* 6, 2229–2237.
  19. Zhang, L., Kang, C., Zhang, G., Pan, Z., Huang, Z., Xu, S., Rao, H., Liu, H., Wu, S., Wu, X., et al. (2020). All-inorganic CsPbI<sub>3</sub> quantum dot solar cells with efficiency over 16% by defect control. *Adv. Funct. Mater.* 31, 2005930.
  20. Hu, L., Zhao, Q., Huang, S., Zheng, J., Guan, X., Patterson, R., Kim, J., Shi, L., Lin, C.H., Lei, Q., et al. (2021). Flexible and efficient perovskite quantum dot solar cells via hybrid interfacial architecture. *Nat. Commun.* 12, 466.
  21. Chen, K., Jin, W., Zhang, Y., Yang, T., Reiss, P., Zhong, Q., Bach, U., Li, Q., Wang, Y., Zhang, H., et al. (2020). High efficiency mesoscopic solar cells using CsPbI<sub>3</sub> perovskite quantum dots enabled by chemical interface engineering. *J. Am. Chem. Soc.* 142, 3775–3783.
  22. Wheeler, L.M., Sanehira, E.M., Marshall, A.R., Schulz, P., Suri, M., Anderson, N.C., Christians, J.A., Nordlund, D., Sokaras, D., Kroll, T., et al. (2018). Targeted ligand-exchange chemistry on cesium lead halide perovskite quantum dots for high-efficiency photovoltaics. *J. Am. Chem. Soc.* 140, 10504–10513.
  23. Sanehira, E.M., Marshall, A.R., Christians, J.A., Harvey, S.P., Ciesielski, P.N., Wheeler, L.M., Schulz, P., Lin, L.Y., Beard, M.C., and Luther, J.M. (2017). Enhanced mobility CsPbI<sub>3</sub> quantum dot arrays for record-efficiency, high-voltage photovoltaic cells. *Sci. Adv.* 3, eaao4204.
  24. Kim, J., Cho, S., Dinic, F., Choi, J., Choi, C., Jeong, S.M., Lee, J.S., Voznyy, O., Ko, M.J., and Kim, Y. (2020). Hydrophobic stabilizer-anchored fully inorganic perovskite quantum dots enhance moisture resistance and photovoltaic performance. *Nano Energy* 75, 104985.
  25. Khan, J., Zhang, X.L., Yuan, J.Y., Wang, Y., Shi, G.Z., Patterson, R., Shi, J.W., Ling, X.F., Hu, L., Wu, T., et al. (2020). Tuning the surface-passivating ligand anchoring position enables phase robustness in CsPbI<sub>3</sub> perovskite quantum dot solar cells. *ACS Energy Lett.* 5, 3322–3329.
  26. Li, X.Y., Zhao, Y.B., Fan, F.J., Levina, L., Liu, M., Quintero-Bermudez, R., Gong, X.W., Quan, L.N., Fan, J.Z., Yang, Z.Y., et al. (2018). Bright colloidal quantum dot light-emitting diodes enabled by efficient chlorination. *Nat. Photonics* 12, 159–164.
  27. Balazs, D.M., Dirin, D.N., Fang, H.H., Protesescu, L., ten Brink, G.H., Kooi, B.J., Kovalenko, M.V., and Loi, M.A. (2015). Counterion-mediated ligand exchange for PbS colloidal quantum dot superlattices. *ACS Nano* 9, 11951–11959.
  28. Song, J.H., Choi, H., Kim, Y.H., and Jeong, S. (2017). High performance colloidal quantum dot photovoltaics by controlling Protic solvents in ligand exchange. *Adv. Energy Mater.* 7, 1700301.
  29. Hassinen, A., Moreels, I., De Nolf, K., Smet, P.F., Martins, J.C., and Hens, Z. (2012). Short-chain alcohols strip X-type ligands and quench the luminescence of PbSe and CdSe quantum dots, acetonitrile does not. *J. Am. Chem. Soc.* 134, 20705–20712.
  30. Kirmani, A.R., Carey, G.H., Abdelsamie, M., Yan, B., Cha, D., Rollny, L.R., Cui, X., Sargent, E.H., and Amassian, A. (2014). Effect of solvent environment on colloidal-quantum-dot solar-cell manufacturability and performance. *Adv. Mater.* 26, 4717–4723.
  31. Shan, S., Li, Y., Wu, H., Chen, T., Niu, B., Zhang, Y., Wang, D., Kan, C., Yu, X., Zuo, L., and Chen, H. (2021). Manipulating the film morphology evolution Toward green solvent-processed perovskite solar cells. *SusMat* 1, 537–544.
  32. Katritzky, A.R., Fara, D.C., Yang, H., Tämm, K., Tamm, T., and Karelson, M. (2004). Quantitative measures of solvent polarity. *Chem. Rev.* 104, 175–198.
  33. De Roo, J., De Keukeleere, K., Hens, Z., and Van Driessche, I. (2016). From ligands to binding motifs and beyond: the enhanced versatility of nanocrystal surfaces. *Dalton Trans.* 45, 13277–13283.
  34. Sliz, R., Lejay, M., Fan, J.Z., Choi, M.J., Kinge, S., Hoogland, S., Fabritius, T., García de Arquer, F.P., and Sargent, E.H. (2019). Stable colloidal quantum dot inks enable inkjet-printed high-sensitivity infrared photodetectors. *ACS Nano* 13, 11988–11995.
  35. Hoshi, K., Chiba, T., Sato, J., Hayashi, Y., Takahashi, Y., Ebe, H., Ohisa, S., and Kido, J. (2018). Purification of perovskite quantum dots using low-dielectric-constant washing solvent "diglyme" for highly efficient light-emitting devices. *ACS Appl. Mater. Interfaces* 10, 24607–24612.
  36. Chiba, T., Hayashi, Y., Ebe, H., Hoshi, K., Sato, J., Sato, S., Pu, Y.J., Ohisa, S., and Kido, J. (2018). Anion-exchange red perovskite quantum dots with ammonium iodine salts for highly efficient light-emitting devices. *Nat. Photonics* 12, 681–687.
  37. Chuang, C.H., Brown, P.R., Bulović, V., and Bawendi, M.G. (2014). Improved performance and stability in quantum dot solar cells Through band alignment engineering. *Nat. Mater.* 13, 796–801.
  38. Lee, J.W., Kim, H.S., and Park, N.G. (2016). Lewis acid-base adduct approach for high efficiency perovskite solar cells. *Acc. Chem. Res.* 49, 311–319.
  39. Jing, Q., Zhang, M., Huang, X., Ren, X.M., Wang, P., and Lu, Z.D. (2017). Surface passivation of mixed-halide perovskite CsPb(Br<sub>1-x</sub>I<sub>x</sub>)<sub>3</sub> nanocrystals by selective etching for improved stability. *Nanoscale* 9, 7391–7396.
  40. Bu, T., Wu, L., Liu, X., Yang, X., Zhou, P., Yu, X., Qin, T., Shi, J., Wang, S., Li, S., et al. (2017). Synergic interface optimization with green solvent engineering in mixed perovskite solar cells. *Adv. Energy Mater.* 7, 1700576.
  41. Marcus, Y. (1993). The properties of organic liquids that are relevant to their use as solvating solvents. *Chem. Soc. Rev.* 22, 409–416.
  42. Krygowski, T.M., Wrona, P.K., Zieleńska, U., and Reichardt, C. (1985). Empirical parameters of lewis acidity and basicity for aqueous binary solvent mixtures. *Tetrahedron* 41, 4519–4527.
  43. Spange, S., Lienert, C., Friebe, N., and Schreiter, K. (2020). Complementary interpretation of  $E_T(30)$  polarity parameters of ionic liquids. *Phys. Chem. Chem. Phys.* 22, 9954–9966.
  44. Han, R., Zhao, Q., Su, J., Zhou, X.J., Ye, X.F., Liang, X.J., Li, J., Cai, H.K., Ni, J., and Zhang, J.J. (2021). Role of methyl acetate in highly reproducible efficient CsPbI<sub>3</sub> perovskite quantum dot solar cells. *J. Phys. Chem. C* 125, 8469–8478.
  45. Wang, Y., Liu, X., Zhang, T., Wang, X., Kan, M., Shi, J., and Zhao, Y. (2019). The role of dimethylammonium iodide in CsPbI<sub>3</sub> perovskite fabrication: additive or dopant? *Angew. Chem. Int. Ed. Engl.* 58, 16691–16696.
  46. Chen, J., and Park, N.G. (2019). Causes and solutions of recombination in perovskite solar cells. *Adv. Mater.* 31, e1803019.
  47. Kim, J., Koo, B., Kim, W.H., Choi, J., Choi, C., Lim, S.J., Lee, J.S., Kim, D.H., Ko, M.J., and Kim,

- Y. (2019). Alkali acetate-assisted enhanced electronic coupling in CsPbI<sub>3</sub> perovskite quantum dot solids for improved photovoltaics. *Nano Energy* 66, 104130.
48. Zeng, Q., Zhang, X., Feng, X., Lu, S., Chen, Z., Yong, X., Redfern, S.A.T., Wei, H., Wang, H., Shen, H., et al. (2018). Polymer-passivated inorganic cesium lead mixed-halide perovskites for stable and efficient solar cells With high open-circuit voltage over 1.3 V. *Adv. Mater.* 30, 1705393.
49. Pan, J., Quan, L.N., Zhao, Y., Peng, W., Murali, B., Sarmah, S.P., Yuan, M., Sinatra, L., Alyami, N.M., Liu, J., et al. (2016). Highly efficient perovskite-quantum-dot light-emitting diodes by surface engineering. *Adv. Mater.* 28, 8718–8725.
50. Wang, S.X., Bi, C.H., Portniagin, A., Yuan, J.F., Ning, J.J., Xiao, X.F., Zhang, X.Y., Li, Y.Y., Kershaw, S.V., Tian, J.J., and Rogach, A.L. (2020). CsPbI<sub>3</sub>/PbSe heterostructured nanocrystals for high-efficiency solar cells. *ACS Energy Lett.* 5, 2401–2410.
51. Yang, F., Chen, H., Zhang, R., Liu, X., Zhang, W., Zhang, J., Gao, F., and Wang, L. (2020). Efficient and spectrally stable blue perovskite light-emitting diodes based on potassium passivated nanocrystals. *Adv. Funct. Mater.* 30, 1908760.
52. Koole, R., Liljeroth, P., de Mello Donega, C., Vanmaekelbergh, D., and Meijerink, A. (2006). Electronic coupling and exciton energy transfer in CdTe quantum-dot molecules. *J. Am. Chem. Soc.* 128, 10436–10441.
53. Wang, Y., Yuan, J., Zhang, X., Ling, X., Larson, B.W., Zhao, Q., Yang, Y., Shi, Y., Luther, J.M., and Ma, W. (2020). Surface ligand management aided by a secondary amine enables increased synthesis yield of CsPbI<sub>3</sub> perovskite quantum dots and high photovoltaic performance. *Adv. Mater.* 32, e2000449.
54. Li, J., Xu, L., Wang, T., Song, J., Chen, J., Xue, J., Dong, Y., Cai, B., Shan, Q., Han, B., and Zeng, H. (2017). 50-Fold EQE improvement up to 6.27% of solution-processed all-inorganic perovskite CsPbBr<sub>3</sub> QLEDs via surface ligand density control. *Adv. Mater.* 29, 1603885.
55. Chiba, T., Hoshi, K., Pu, Y.J., Takeda, Y., Hayashi, Y., Ohisa, S., Kawata, S., and Kido, J. (2017). High-efficiency perovskite quantum-dot light-emitting devices by effective washing process and interfacial energy level alignment. *ACS Appl. Mater. Interfaces* 9, 18054–18060.
56. Zheng, X.P., Chen, B., Dai, J., Fang, Y.J., Bai, Y., Lin, Y.Z., Wei, H.T., Zeng, X.C., and Huang, J.S. (2017). Defect passivation in hybrid perovskite solar cells using quaternary ammonium halide anions and cations. *Nat. Energy* 2, 17102.
57. Wang, Y., Dar, M.I., Ono, L.K., Zhang, T., Kan, M., Li, Y., Zhang, L., Wang, X., Yang, Y., Gao, X., et al. (2019). Thermodynamically stabilized beta-CsPbI<sub>3</sub>-based perovskite solar cells with efficiencies >18%. *Science* 365, 591–595.
58. Wang, J., Liu, Y., Zhou, Z.N., Fu, Y., and Chang, J. (2017). Epoxidation of soybean oil catalyzed by deep eutectic solvents based on the choline chloride–carboxylic acid bifunctional catalytic system. *Ind. Eng. Chem. Res.* 56, 8224–8234.
59. Ge, Y., Mu, X.L., Lu, Y., and Sui, M.L. (2020). Photoinduced degradation of lead halide perovskite thin films in air. *Acta Phys. Chim. Sin.* 36, 1905039.
60. Guo, Z., Jena, A.K., Takei, I., Kim, G.M., Kamarudin, M.A., Sanehira, Y., Ishii, A., Numata, Y., Hayase, S., and Miyasaka, T. (2020).
- V<sub>OC</sub> over 1.4 V for amorphous tin-oxide-based dopant-free CsPbI<sub>2</sub>Br perovskite solar cells. *J. Am. Chem. Soc.* 142, 9725–9734.
61. Li, X., Fu, S., Zhang, W., Ke, S., Song, W., and Fang, J. (2020). Chemical anti-corrosion strategy for stable inverted perovskite solar cells. *Sci. Adv.* 6, eabd1580.
62. Zai, H.C., Su, J., Zhu, C., Chen, Y.H., Ma, Y., Zhang, P.X., Ma, S., Zhang, X., Xie, H.P., Fan, R.D., et al. (2021). Sandwiched electrode buffer for efficient and stable perovskite solar cells with dual back surface fields. *Joule* 5, 2148–2163.
63. Jia, D., Chen, J., Zheng, S., Phuyal, D., Yu, M., Tian, L., Liu, J., Karis, O., Rensmo, H., Johansson, E.M.J., and Zhang, X. (2019). Highly stabilized quantum dot ink for efficient infrared light absorbing solar cells. *Adv. Energy Mater.* 9, 1902809.
64. Zhang, X., Zhang, J., Phuyal, D., Du, J., Tian, L., Öberg, V.A., Johansson, M.B., Cappel, U.B., Karis, O., Liu, J., et al. (2018). Inorganic CsPbI<sub>3</sub> perovskite coating on PbS quantum dot for highly efficient and stable infrared light converting solar cells. *Adv. Energy Mater.* 8, 1702049.
65. Jayasree, E.G., and Sreedevi, S. (2020). A DFT study on Protic solvent assisted tautomerization of heterocyclic thiocarbonyls. *Chem. Phys.* 530, 110650.
66. Liptak, M.D., and Shields, G.C. (2001). Accurate pK<sub>a</sub> calculations for carboxylic acids using complete basis set and Gaussian-n models combined with CPCM continuum solvation methods. *J. Am. Chem. Soc.* 123, 7314–7319.